213
12/30/81
(8B)

(2)

MASTER

DR. 182

SERI/PR-0-9372-2
(DE81030278)

AMORPHOUS SILICON SOLAR CELLS

Quarterly Report No. 2 for the Period January 1—March 31, 1981

By
D. E. Carlson
R. S. Crandall
J. Dresner
B. Goldstein
J. J. Hanak
A. R. Moore
H. E. Schade
D. L. Staebler
H. A. Weakliem
R. Williams

May 1981

Work Performed Under Contract No. AC02-77CH00178

Solar Energy Research Institute
Golden, Colorado

U.S. Department of Energy

Solar Energy

SERI/PR-0-9372-2
(DE81030278)
Distribution Category UC-63

SERI/PR-0-9372-2
UC Category, UC-63

SERI/PR--0-9372-2

DE81 030278

AMORPHOUS SILICON SOLAR CELLS

Quarterly Report No. 2
for the period 1 January 1981 to
31 March 1981

May 1981

D. E. Carlson, R. S. Crandall, J. Dresner,
D. Goldstein, J. J. Hanak, A. R. Moore, H. E. Schade,
D. L. Staebler, H. A. Weakliem, and R. Williams

RCA Laboratories
Princeton, New Jersey 08540

Prepared Under Subcontract
No. XG-0-9372-1
for the

Solar Energy Research Institute
A Division of Midwest Research Institute
1536 Cole Boulevard
Golden, Colorado 80401

PREFACE

This Quarterly Report covers the work performed by the Display and Energy Systems Research Laboratory of RCA Laboratories, Princeton, New Jersey, for the period 1 January 1981 to 31 March 1981 under Contract No.XG-0-9372-1. The Staff Vice President is B. F Williams; D. E. Carlson is the Group Head and Project Scientist. The staff members and associate staff personnel who have contributed to the report, and their areas of specialization, are listed below.

D. E. Carlson R. W. Smith	dc Deposition of a-Si:H
*R. S. Crandall J. A. Cioppi	Device Modeling, DLTS
*J. Dresner	Diffusion-Length Measurements
*A. R. Moore	Diffusion-Length Measurements
*B. Goldstein D. J. Szostak	Diffusion-Length Measurements
†J. J. Hanak J. P. Pellicane V. Korsun	rf-Deposition of a-Si:H; Structures; Stability Studies
†J. I. Pankove J. E. Berkeyheiser	Photoluminescence
*H. E. Schade	Electron-Radiation Damage in a-Si:H; Interface Studies
*D. L. Staebler G. R. Latham	Stability Studies
*H. A. Weakliem A. V. Cafiero	Optical-Emission Spectroscopy; rf-Doping Studies
†R. Williams	Interface Studies; Device Modeling

---

*Member of Technical Staff
†Fellow

SUMMARY

An analysis of the photoconductive response of Schottky-barrier and p-i-n solar cell structures shows that the photoconductivity determines the fill factor, rather than the dark current, as in crystalline silicon cells. An analysis of the I-V curves of p-i-n cells shows that the electron and hole drift lengths are comparable.

High-conductivity p- and n-type films ($\sigma \approx 1\text{-}10\ \Omega^{-1}\cdot\mathrm{cm}^{-1}$) have been produced in an rf discharge for $T_s > 400°\mathrm{C}$ and in a dc cathodic discharge for $T_s > 350°\mathrm{C}$. Some of these high-conductivity films are clearly microcrystalline, while others appear to be still amorphous.

Diffusion lengths of $\sim$0.8 μm have been measured in undoped a-Si:H films at illumination levels of $\sim$0.1 Sun. The activation energy of the diffusion length is $\sim$0.28 eV. The technique for measuring the diffusion length has been improved by means of a liquid Schottky-barrier contact.

Preliminary results confirm that carbon alloying of the p layer improves the performance of p-i-n cells illuminated through that layer. Tests on p-i-n cells with ITO contacts on both sides show that the stability is better for cells illuminated through the p layer. A statistical analysis of solar-cell data indicates that a major factor determining the efficiency of ITO/n-i-p cells is the ITO/n contact.

We have determined several parameters that affect device stability. A gradual boron profile enhances stability, as does a thin, undoped layer. Increased oxygen contamination increases the degradation of a-Si:H p-i-n cells.

TABLE OF CONTENTS

SECTION PAGE

TABLE OF CONTENTS (Continued)

SECTION PAGE

APPENDICES

LIST OF FIGURES

LIST OF FIGURES

LIST OF TABLES

SECTION 1.0

INTRODUCTION

A review of the history of hydrogenated amorphous silicon (a-Si:H) and the a-Si:H solar cell can be found in Ref. 1. The present program involves six research tasks: theoretical modeling, deposition and doping studies, experimental methods for the characterization of a-Si:H, formation of solar-cell structures, theoretical and experimental evaluation of solar-cell parameters, and stability studies.

In a separate program, researchers at RCA Laboratories are developing the technology to fabricate large-area a-Si:H solar cells. This program has the objective of developing low-cost, large-area a-Si:H solar panels.

SECTION 2.0

THEORETICAL MODELING: COMPARISON OF p-i-n AND SCHOTTKY-BARRIER a-Si:H SOLAR CELLS

2.1 INTRODUCTION

A promising material for solar-cell applications is hydrogenated amorphous silicon, a-Si:H. Thin-film solar cells with efficiencies greater than 6% have been fabricated from this material [1-3]. Both Schottky-barrier and p-i-n cells give high efficiency. Nevertheless, the p-i-n structure appears to give the highest efficiency for large-area cells [2]. Some of the reasons why the p-i-n structure may ultimately make the best solar cell are presented in the following paragraphs. These are discussed within the framework of the factors that determine its efficiency. Generally, these can be represented by the fill factor (FF), short-circuit current (I_{sc}), and the open-circuit voltage (V_{oc}). It is the electron and hole transports that determine the fill factor; i.e., essentially the shape of the current-voltage curve. These play a lesser role in determining the short-circuit current and an even smaller role in determining the open-circuit voltage.

The a-Si:H-based cell is different from the usual crystalline solar cell, where diffusion of electron-hole pairs from the low-field bulk region to the high-field junction is the main source of the photocurrent. Since the electron-hole pair diffusion length in a-Si:H is short [4], the collected current comes from those electron-hole pairs that are formed in the high-field junction region. Thus, both the transport in this region, as well as the width of the region, determine the collection efficiency. The best cells will be those in which the electric field extends throughout the entire intrinsic region.

Measurements of the voltage dependence of the photocurrent for both Schottky-barrier and p-i-n structures are presented first; the results in terms of simplified models of the two structures are then compared.

2.2 EXPERIMENTAL DETAILS

Results of photocurrent measurements on two types of thin-film solar cells produced by dc glow-discharge decomposition of silane on heated substrates of stainless steel are presented next. Cells produced by rf discharge on other substrates show similar properties. The Schottky-barrier cell was made by first depositing a few-hundred-Å a-Si:H layer doped with phosphorus, followed by an undoped layer [5]. A thin layer of platinum formed the Schottky-barrier contact. The p-i-n structure was grown by first depositing a thin boron-doped layer on the stainless steel, then following this with an undoped layer, and finally adding a thin phosphorus-doped layer. The conducting transparent layer to the n-type phosphorus contact was electron-beam-evaporated ITO*.

Photocurrent measurements were made with chopped light at frequencies low enough that long response times did not limit the measurements. The light source was a krypton laser, tuned to 674 nm. The absorption spectrum of a-Si:H is such that light of this wavelength is nearly uniformly absorbed.

Figure 2-1 shows the photocurrent as a function of bias applied to a p-i-n solar cell illuminated with uniformly absorbed light through the n contact. Here, and throughout this discusssion, photocurrent, by definition, is the difference between the current under illumination with weakly absorbed light and the current in the dark. For negative voltage the photocurrent saturates at sufficiently large reverse bias. For positive bias the photocurrent decreases and changes sign at a bias V_f. The positive photocurrent usually is referred to as a primary photocurrent, because the contacts are blocking for the photoexcited carriers. The negative photocurrent is referred to as a secondary photocurrent, because the contacts are, in this case, ohmic [6]. The broken curve in Fig. 2-1 shows the total current (the sum of photocurrent and dark current) for reference purposes. Only at low temperature, where the dark current is zero, would the total current and photocurrent coincide. It is evident from the figure that the magnitude of the dark current is much smaller than that of the photocurrent, except near V_{oc}.
The data in Fig. 2-1 shows that the photocurrent in the vicinity of V_f varies linearly with voltage. This is the region where the photocurrent changes from primary to secondary. An important point here is that the magnitude of the slope of the photocurrents-vs-voltage curve is the same for primary and secondary photocurrents. This implies that the transport mechanisms are the same

---

*Indium-tin-oxide transparent contact.

for either type of photocurrent in the vicinity of V_f. The linear slopes show that the photocurrents obey Ohm's law.

In Fig. 2-2 the photocurrent for a Schottky-barrier cell is shown for illumination through the platinum Schottky-barrier contact with weakly absorbed light. The broken curve in the figure shows the photocurrent on an expanded voltage scale in the vicinity of V_f. In this case, in contrast to the result in Fig. 2-1 for the p-i-n structure, the primary photocurrent is not ohmic.

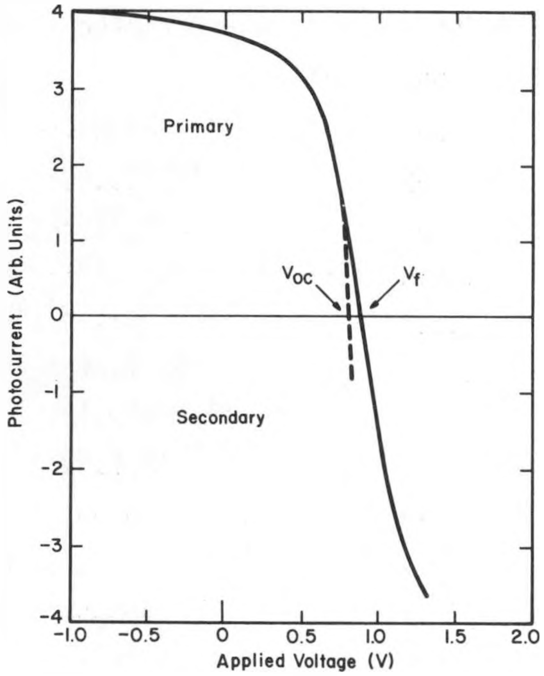

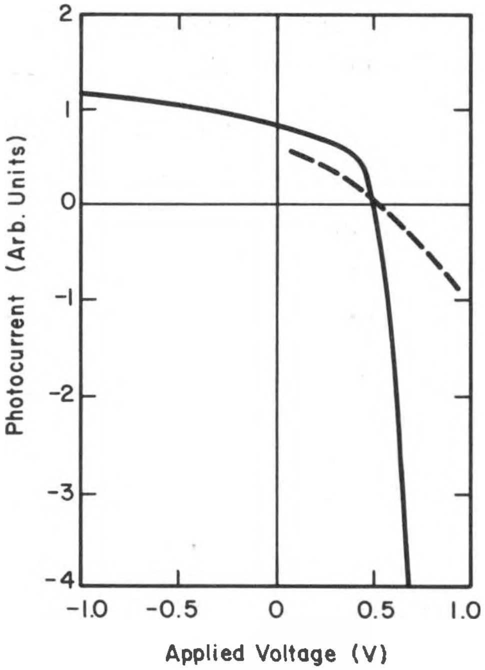

Figure 2-1. PHOTOCURRENT OF A p-i-n SOLAR CELL vs VOLTAGE FOR ILLUMINATION WITH 674-nm LIGHT AT ROOM TEMPERATURE (The dotted curve is the dark current.)

Figure 2-2. PHOTOCURRENT OF A SCHOTTKY-BARRIER SOLAR CELL AS A FUNCTION OF CELL BIAS (Experimental conditions are the same as in Figure 2-1. The dashed curve is for a voltage scale expansion of ten.)

2.3 DISCUSSION

2.3.1 Schottky-Barrier Cell

There is a simple reason for the nonohmic nature of the primary photocurrent in the Schottky-barrier structure. This becomes apparent in Fig. 2-3, where the equilibrium potential-energy diagram is sketched. The Fermi level near the Schottky-barrier contact lies well below midgap in the region of the high density of valence-band states [7]. In the process of forming this metal-semiconductor contact, the Fermi level must move from near midgap to well below midgap. To accommodate this, electrons leave the i layer, producing a large density of positive charge in the region within a depletion width of the Pt/a-Si:H interface. This charge leads to a decrease in the electric field with distance from the Pt contact. Since the electron-hole pair diffusion length is low, pairs created in the low-field region will have little chance of being separated before they recombine and thus will not be collected at the contacts. Electron-hole pairs produced in the high-field region have the best chance of being collected at the contacts. Therefore, the photocurrent will be proportional to the width of the high-field region. For the Schottky barrier discussed here, the width of the high-field region can be described by the classical depletion-width model [8], in which the depletion width is proportional to the square root of voltage across the sample.

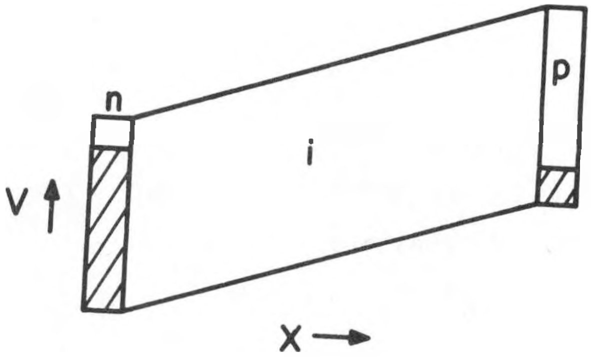

Figure 2-3. ELECTRON POTENTIAL-ENERGY DIAGRAM FOR A SCHOTTKY-BARRIER SOLAR CELL MADE OF n-TYPE a-Si:H

Evidence for this model is shown in Fig. 2-4, where the reciprocal of the square of the capacitance is plotted vs applied voltage. For a Schottky barrier, the curve should be a straight line, as shown in the figure. These measurements were made at 100 Hz, but similar results were obtained between 10 and 50 kHz. The illumination intensity corresponds to 16 mW cm^{-2}.

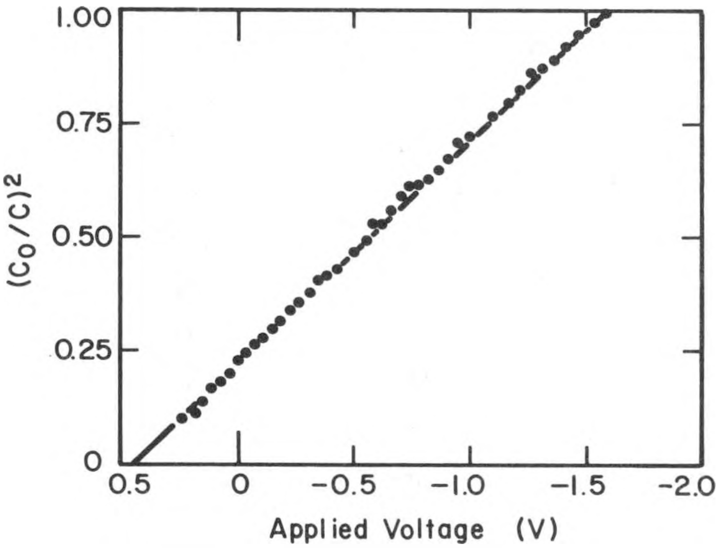

Figure 2-4. RECIPROCAL OF THE SQUARE OF THE CAPACITANCE vs BIAS FOR A SCHOTTKY-BARRIER SOLAR CELL (The measuring frequency is 100 Hz; the cell is illuminated with 16 mW/cm^2 674-nm light.)

Figure 2-5 shows the photocurrent as a function of the depletion width, W. It was determined from the capacitance measurements. The conditions are the same as in Fig. 2-4. Except for the small region near the minimum depletion width, the current varies linearly with the depletion width, consistent with the model that only carriers produced in this region are collected. Since the current varies linearly with the depletion width, and the depletion width varies as the square root of the voltage, the current also varies as the square root of the depletion width. This is in contrast to the p-i-n cell, where the photocurrent obeys Ohms law near V_f. The fact that the line does not extrapolate through the origin, but rather has an intercept at finite depletion width, has been interpreted in terms of geminate recombination [9].

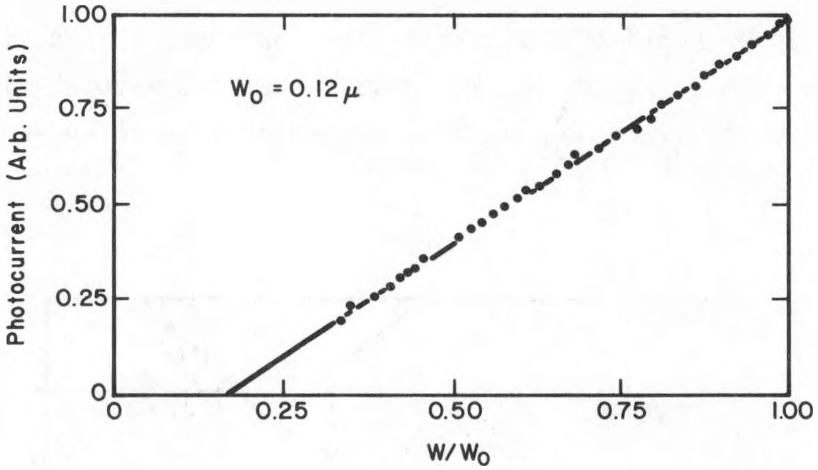

Figure 2-5. PHOTOCURRENT vs DEPLETION WIDTH FOR THE SCHOTTKY-BARRIER SOLAR CELL (Under the conditions given for Fig. 2-4.)

The secondary photocurrent, on the other hand, is ohmic as expected, since for applied voltages greater than V_f, the electric field extends throughout the thickness of the a-Si:H film.

2.3.2 Solar Cell

To describe the transport in the p-i-n structure we refer to the idealized potential-energy diagram in Fig. 2-6. This figure is similar to that for the Schottky-barrier structure shown in Fig. 2-3 with one important exception: the potential varies nearly linearly across the i layer because there is little space charge in the i layer. This occurs because of the growth procedure. The solar cell is grown with the p layer put down first, followed by the i layer. Because the discharge is not terminated and all the boron is not purged from the system, there is residual boron in the i layer. The boron concentration decreases from the p side toward the n side, resulting in an i layer that is graded p to n type. This has an important effect on the behavior of the solar cell. It produces an i layer that contains much less space charge than the Schottky-barrier cell. The majority of the space charge resides in the depletion widths in the n and p contacts. Thus one can reasonably approximate the field in the i layer as being uniform, simplifying the analysis of the transport data.

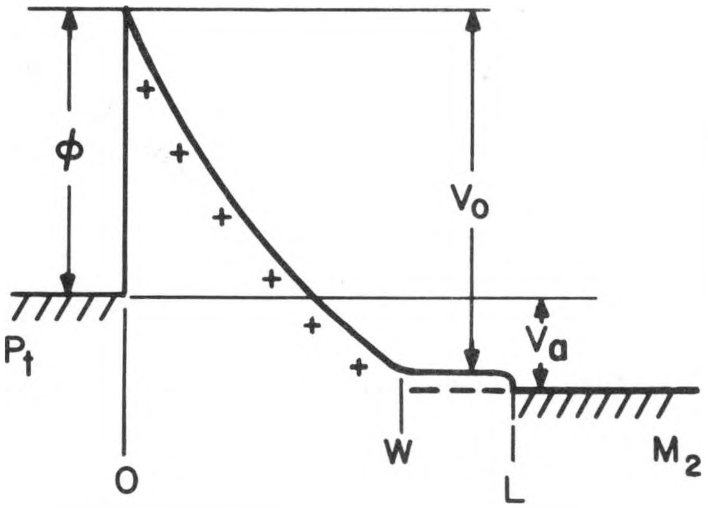

Figure 2-6. POTENTIAL ENERGY DIAGRAM FOR A p-i-n SOLAR CELL (The n and p layers contain the space charge that is necessary to support the uniform field in the i layer.)

Support for this model of the p-i-n structure is given by capacitance-voltage measurements. For the model of the p-i-n structure with all the space charge contained in the n and p layers, the derivation in Appendix A shows that the depletion width (reciprocal of the capacitance) varies linearly with voltage. Therefore, the capacitance-voltage data are presented in Fig. 2-7 to emphasize this behavior. The measurements were made at 250 K to minimize the contribution from the diffusion capacitance in forward bias [10]. The data in the figure clearly exhibit this linear dependence of the depletion width on bias. The depletion width of the p-i-n structure changes by only 3% over the large voltage range, because it is the depletion widths in the n and p contacts, which are a small fraction of the i-layer thickness, that change with voltage. These results are not consistent with recent proposals [11] that the best description of the potential in the i layer in the p-i-n structure is that of two Schottky barriers in series. For this case the capacitance should vary as the square root of the voltage and furthermore there would be large changes in the capacitance with voltage, as for the Schottky-barrier cell.

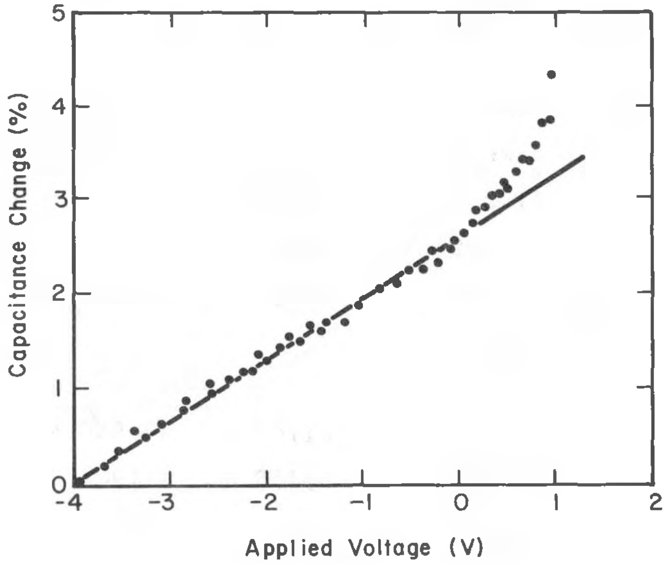

Figure 2-7. RECIPROCAL OF CAPACITANCE vs BIAS FOR A p-i-n SOLAR CELL

If we take the above capacitance-voltage results as evidence that the p-i-n structure can be described by a uniform field throughout the i layer, then the voltage dependence of the photocurrent can be understood in terms of a simple model of the transport in this cell. For the linear portion of the current-voltage curve shown in Fig. 2-1, both the primary (positive) and secondary (negative) photocurrents must be described by Ohm's law. The photocurrent is therefore,

$$J = e(nv_n + pv_p) = eG(l_n + l_p) \quad , \qquad (2\text{-}1)$$

where e is the magnitude of the electron charge, n the density of photo-excited electrons per unit volume, and v_n the electron-drift velocity; the quantities p and v_p have similar definitions for the holes. The quantity G is the number of electron-hole pairs produced per unit volume per unit time. The second expression follows from the definitions of the drift length and lifetime. The electron and hole drift lengths (mean distance traveled in the direction of the field before recombination) are, respectively,

$$l_n = v_n \tau_n \, , \quad l_p = v_p \tau_p \quad . \qquad (2\text{-}2)$$

The times τ_n and τ_p are, respectively, the lifetimes of the electron and hole before recombining. The free electron and hole densities, in the steady state, are given by

$$n = G\tau_n \ , \quad p = G\tau_p \ . \tag{2-3}$$

The fact that the current-voltage curves have the same slope on either side of V_f implies that the transport parameters do not change as the electric field in the i layer changes sign. Since the contacts do not determine the transport at low fields, it is determined by recombination in the bulk.

The photocurrent given by Eq. 2-1 is just the usual photocurrent that would be measured on a bulk film with ohmic contacts. This type of measurement is often used as a guide to the quality of the photoconductor and to the nature of the recombination centers [7,12,13]. In a-Si:H one usually finds that the recombination centers are distributed in energy [12,13]. The evidence for this is that the photocurrent exhibits a power-law variation with light intensity where the power is between 0.5 and 1.0 [6]. Typical values for a-Si:H are between 0.7 and 0.8 [12,13]. The photocurrent in the p-i-n structure, on the other hand, shows a linear variation of photocurrent with light intensity typical of a single recombination center. The photocurrent versus light intensity for the p-i-n structure is shown in Fig. 2-8. Here the logarithm of the photocurrent is plotted versus the logarithm of the light intensity. The slope of the line through the data points is unity. As the electric field increases, the sum of the electron and hole drift lengths will increase until they are on the order of the i-layer thickness (L). Then the contacts, which are blocking for this primary photocurrent, will limit the current flow, reducing it below the Ohm's-law value. When the sum of these drift lengths significantly exceeds the i-layer thickness, the current saturates at a value eGL.

This concept is aided by reference to Fig. 2-9 which is a sketch of the electron and hole densities in the i layer for the condition where $\ell_p + \ell_n < L$. In this case, strong recombination in the bulk of the i layer keeps the carrier density constant in this region. The electron and hole densities are thus given by Eq. 2-3. The lifetimes are constants, independent of position. Near the blocking contacts this approximation breaks down within a distance approximating the minority-carrier drift length. Near the n-i interface this length

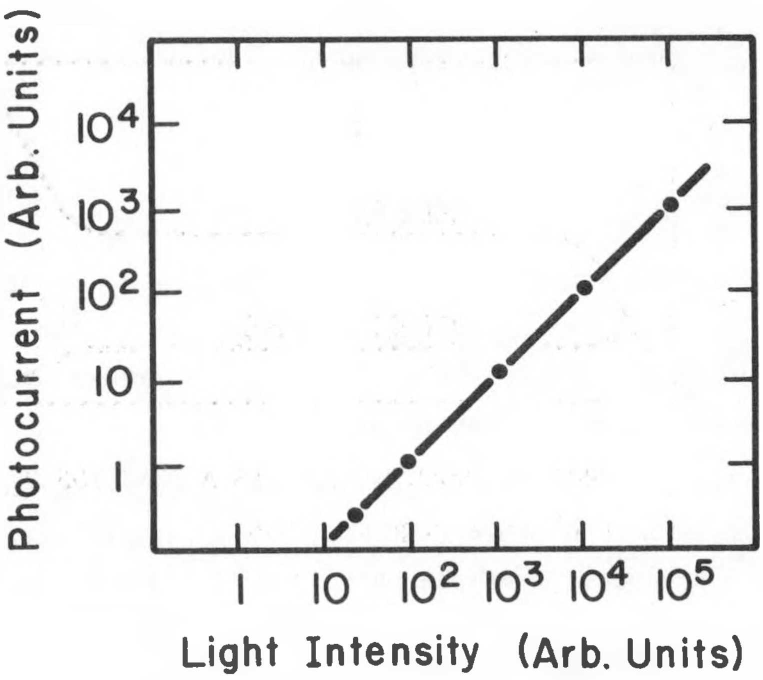

Figure 2-8. LOGARITHM OF THE PHOTOCURRENT vs LIGHT INTENSITY, WITH 674-nm LIGHT (Measurements were made on a p-i-n cell in the Ohm's-law region near V_f. The maximum light intensity is about 120 mW/cm^2 incident on the cell.)

is the drift length of the minority-carrier holes, and at the i-p interface it is the drift length of the minority-carrier electrons. Since there is no recombination in these regions, the electron and hole densities increase linearly as a function of position.

To make an exact calculation of the detailed shape of the photocurrent-voltage curve in the transition region between the Ohm's-law and saturated-current regions requires a numerical solution of the continuity equation, as well as a detailed knowledge of the spatial dependence of the electron-hole recombination times. Nevertheless, arguments are given in Appendix B for an approximate solution to the continuity equation that agrees quite well with experiment. However, even though a simple expression that connects the Ohm's-law region with the transition region can be obtained, no new physical information is obtained, since the only parameter in the expression for the current, Eq. B-13, is the sum

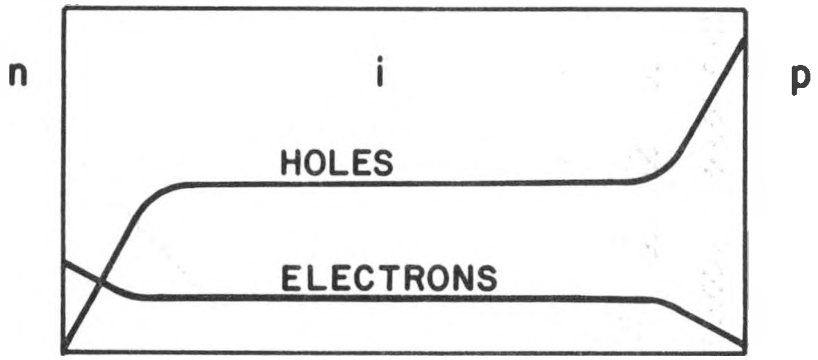

Figure 2-9. ELECTRON AND HOLE DENSITY AS A FUNCTION OF DISTANCE IN THE i LAYER OF A p-i-n CELL

of the electron and hole drift lengths, which can also be determined without a detailed knowledge of the transport, as is outlined next.

From the ohmic and saturated regions of the primary-photocurrent/voltage curve, one can determine the important transport parameters, namely the drift lengths. The saturated value of the photocurrent determines the magnitude of the generation rate, G, independent of any knowledge of the absorption constant or transmission coefficient of the contacts. Dividing G, determined in this manner, into the photocurrent in the ohmic region gives the sum of the electron and hole drift lengths. Even though we cannot separate the sum into its constituents, this is not a drawback for solar-cell operation, because it is the sum of these two that determines the operating parameters for the cell.

Analysis of the data in Fig. 2-1 shows that $\mu_p\tau_p + \mu_n\tau_n = 7 \times 10^9\ cm^2\ V^{-1}$. This number can be compared with estimates of the $\mu\tau$ products determined by other means. Moore [14] has made measurements of the hole-diffusion length, using the PEM effect on thin films of a-Si:H. He finds a diffusion length of about 0.1 μm.

From his data he determined $\mu_p\tau_p = 3.2 \times 10^{-9}\ cm^2/V$. Substituting this value into the sum of the $\mu\tau$ products determined above, we find that $\mu_n\tau_n \approx 3.8 \times 10^{-9}\ cm^2/V$, on the same order as the $\mu\tau$ product for holes. This is a surprising result, since it is generally believed that the hole drift length is much longer than the electron-drift length. Also, Moore [14] found the at $\mu_n\tau_n = 7.8 \times 10^{-8}$ cm^2/V, about 20 times the value found for the p-i-n cell. The difference may be a property of the p-i-n cell, in that the i layer is presumably different from the material studied by Moore because of the residual boron in the i layer of the p-i-n cell.

SECTION 3.0

DEPOSITION AND DOPING STUDIES

3.1 rf-DEPOSITION STUDIES: BORON AND PHOSPHORUS DOPING

The large-area rf-diode/magnetron deposition system was used to deposit several boron-doped a-Si:H films from both SiH_4 and SiH_4/H_2 discharges under various discharge conditions: total pressure, $[H_2]/[SiH_4]$ ratio, rf power, substrate temperature, but a fixed $[B_2H_6]/[SiH_4]$ ratio of 0.01. In most cases, the resistivity of the films was of the order of 1000 Ω-cm, however, two films deposited at a substrate temperature of 410 ± 15°C had resistivities in the range from 1 to 10 Ω-cm. Electron-diffraction measurement of these films (by J. McGinn*) showed them to be amorphous (a crystallite size less than 25 Å). Composition analysis using SIMS (E. Botnick and C. W. Magee*) showed boron concentrations ranging from 0.4 to 1.1% and hydrogen concentrations ranging from ∿1 to 4%. The incorporation in the film of boron concentrations equal to or slightly less than the $[B_2H_6]/[SiH_4]$ ratio in the gas phase is in distinct contrast to results found earlier for a dc(p) discharge, where 2 to 3 times more boron were incorporated into the films than was present in the gas phase.

The optical absorption spectra of the boron-doped films have shapes similar to those of undoped a-Si:H films and show the same red shift with increasing substrate temperature. The spectra of these boron-doped a-Si:H films are reasonably well approximated by a 0.25 eV rigid red shift of the undoped a-Si:H spectra.

Two P-doped films were also deposited on a substrate having a temperature gradient of 200 to 400°C from a 10% (SiH_4 + 1% PH_3), 90% H_2 rf(c) discharge. The films at the hot end have conductivities between 0.03 and 0.2 ohm^{-1} cm^{-1}; the conductivity at the cooler end ranged to 10^{-3} ohm^{-1} cm^{-1}. The morphology of these films has not yet been examined.

High-conductivity films have been prepared for both B and P doping, but only at substrate temperatures above 400°C. We have been unable to prepare high-conductivity films at low-substrate temperatures, although we used conditions which

---

*RCA Laboratories.

are thought to be close to those used by Matsuda et al. [15] who reported the preparation of low-substrate-temperature, high-conductivity phosphorus-doped a-Si:H films.

3.2 FILMS PREPARED FROM DISILANE

An undoped a-Si:H film was prepared with disilane in the rf-diode discharge. The conditions used were: p(disilane), 20 mTorr; flow 60, SCCM; rf power, 0.03 W/cm^2. The deposition rate was 150 Å/min, and the film looked clear and adhered well to 7059 glass and c-Si.

The deposition rate found for the disilane discharge was about 25% faster than for a monosilane discharge, under the same discharge conditions. The optical spectrum was found to be quite similar to that of a film prepared from a silane discharge but having a substrate temperature about 25°C higher than that used for disilane deposition. The infrared spectrum shows a single symmetric peak at 2000 cm^{-1} (the Si:H stretch) and some very weak bands near 800 cm^{-1}.

A boron-doped film from a discharge having the gas composition 50 SCCM (1000 ppm B_2H_6 in H_2) and 3.5 SCCM Si_2H_6 was deposited on a substrate having a temperature gradient 220 → 360°C. The resistivity decreased with increasing substrate temperature, but the minimum value found was 5000 Ω-cm. The film was found to contain 0.35% B and 4% H, and the absorption spectrum is quite similar to that of films having similar composition and substrate temperature, but prepared using monosilane.

3.3 ANALYSIS OF THE OPTICAL EMISSION SPECTRA OF SILANE GLOW DISCHARGES

We have measured the optical emission spectra of glow discharges of gases such as SiH_4, $SiH_4 + H_2$, $SiH_4 + N_2$, $SiH_4 + PH_3$, $SiH_4 + B_2H_6$, H_2, N_2, and Ar, with the large (cathode area of 530 cm^2) rf-diode/magnetron glow-discharge deposition system. The spectra were measured with medium resolution (∿5 Å bandwidth). The relatively high scattered light of the monochromator used limited the detection of weak emission lines from 10^{-5} to 10^{-4} times the intensity of the strong lines.

In a pure silane discharge one observes emission from SiH (predominant band at 414 nm), Si (lines observed at 288 and 390.5 nm), H_2 (which has no really dominant lines but covers the entire UV-VIS-IR spectrum), and the Balmer Lines of H (H_α = 656 nm, H_β = 486 nm, H_γ = 434 nm, and H_δ = 410 nm). The SiH molecule has very high vibrational and rotational temperatures (1000-2000 K) which may be deduced from analysis of the band shape.

The emission spectra are rather complicated in detail, but the principal conclusions of our preliminary spectral analysis of silane discharges can be summarized as follows: high silane flow and low rf power favors the production of SiH and Si, whereas high power and low flow favors production of H and H_2; the operating pressure strongly influences the relative excitation efficiency of the emission lines, probably as a result of the strong dependence of the electron temperature and distribution function on pressure, particularly in the low-pressure region.

We can readily detect the PH-emission lines in a 1% PH_3 + 99% SiH_4 discharge, but have not observed the much weaker emission from boron-hydride species in a 1% B_2H_6 + 99% SiH_4 discharge. Our present apparatus, however, does not permit the detection of trace impurities like O_2 and N_2 in a SiH_4 discharge by the observation of the characteristic N_2, SiN, and SiO emission bands because of the relatively high scattered-light intensity.

The intensity distribution among the atomic-hydrogen Balmer lines is different for a silane discharge than for a hydrogen discharge. The relative intensities of the emitting species SiH, Si, H_2, and H all depend on the discharge parameters: pressure, flow, and rf power. The dependence is, in general, different for each species. We are studying this dependence by comparison of the intensities with that of the characteristic N_2 emission lines, where a fixed fraction of N_2 has been added to the discharge. We will report on the results of this study in Quarterly Report No. 3.

3.4 MASS SPECTROSCOPY

The mass spectrometer was removed from the discharge chamber for cleaning and repair. We completed the design of a chamber to contain a tuning-fork modulator and an electrostatic focussing lens. The modulator will enable us to measure the mass spectrum of the neutral molecules effusing through the aperture from the plasma chamber without interference from the neutrals of the residual gas in the mass-spectrometer chamber. The lens system is being added in order to extract ions from the plasm more efficiently and to increase the detection sensitivity of the apparatus. We expect to have the mass spectrometer (with the modulator chamber attached) in operation within a few weeks.

3.5 DEPOSITION OF SnO_x FILMS FROM A dc GLOW DISCHARGE

The deposition of SnO_x films on 7059 glass substrates was made in a dc glow discharge using the proximity mode. $Sn(CH_3)_4$ having a purity of 99.5% was mixed with 85% O_2 and 1% HF at a pressure of 0.75 Torr, and the discharge was operated at a current density of 0.5 mA/cm^2. The substrate temperature was 300°C and the flow rate, ~30 SCCM. These conditions were found to be optimum and the SnO_x films thus prepared had a resistivity of 2×10^{-2} Ω-cm, a thickness of 1100 Å, and a transparency of >80% over the wavelength range of 4000-7500 Å.

SnO_x films will be prepared from electronic grade $Sn(CH_3)_4$ with a purity of 99.999% and several runs will be made under the above conditions in an attempt to lower the resistivity of the SnO_x films still further.

3.6 HIGH-CONDUCITIVTY FILMS: dc DEPOSITION

Recently, several investigators reported obtaining high-conductivity films ($\sigma > 1\ \Omega^{-1}cm^{-1}$) using glow discharges in atmospheres such as 30% SiH_4 in H_2 [15]; 10% SiH_4 in Ar [16]; 10% SiH_4 in He [17]; and 90% SiF_4, 10% H_2 [15]. In all cases, these films were shown to be partially microcrystalline by means of electron-diffraction analysis [17] or x-ray-diffraction analysis [15,16].

The objective of the present study was to investigate the conditions for forming microcrystalline Si:H films (m-Si:H) from dc cathodic discharges in atmospheres containing SiH_4 diluted in H_2. Most of the work in the present study used SiH_4 that had been premixed with 1.3% B_2H_6, but some films were also made using SiH_4 containing 1% PH_3. Usually, the pressure was 2.5 Torr and the flow rate was ~100 SCCM. The current density at the cathodic substrate was typically 0.55 mA/cm^2 with an applied voltage of ~620V. The films were generally deposited on an SiO_2 substrate containing a multitude of Mo or Cr stripes.

Figure 3-1 shows how the conductivity varied for a film grown at 400°C in a discharge containing 3.5% SiH_4 (1.3% B_2H_6) in H_2. The gas-flow geometry is shown in the inset. These data show that the formation of the high-conductivity region depends on the location of the substrate with respect to the gas-flow inlet. One possible explanation of the results shown in Fig. 3-1 is that gas-phase nucleation tends to inhibit the formation of m-Si:H films (the longer reactive species stay in the discharge, the more likely gas-phase nucleation or polymerization is to occur).

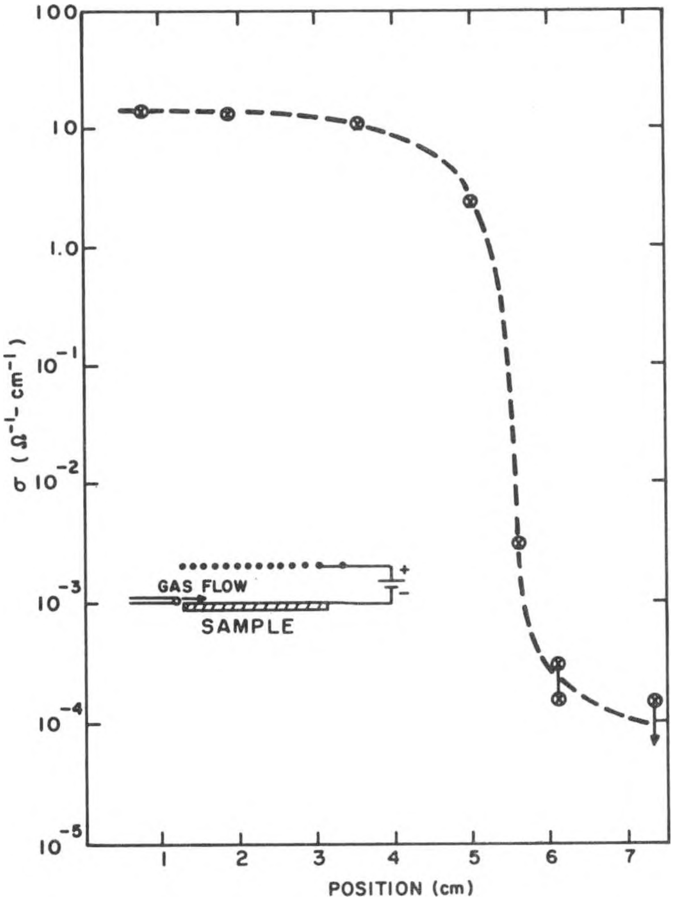

Figure 3-1. CONDUCTIVITY AS A FUNCTION OF POSITION FROM THE GAS INLET FOR A FILM GROWN IN A dc CATHODIC DISCHARGE (The gas was introduced from a horizontal tube near one end of the sample-see inset.)

In another series of experiments, the films were deposited on substrates in a temperature gradient, so that the transition temperature (T_c) between the amorphous and microcrystalline regions could be determined. Figure 3-2 shows that the composition of the discharge atmosphere can affect the value of T_c. For a discharge in 5% SiH (1% PH_3) in H_2, $T_c \approx 382°C$ (curve A) while for 5% SiH_4 (1.3% B_2H_6) in H_2, $T_c \approx 400°C$ (not shown). Adding 10% Ar to the atmosphere in the last case increases T_c to $\sim$420°C (curve B). Replacing SiH_4 with Si_2H_6 causes T_c to increase from $\sim$400 to $\sim$465°C (curve C). Replacing H_2 with He for 9% SiH_4 (1.3% B_2H_6) causes T_c to increase from $\sim$370°C (not shown) to $\sim$515°C (curve D).

The increase in T_c upon replacing SiH_4 with Si_2H_6 supports the hypothesis made earlier that gas-phase nucleation inhibits the formation of m-Si:H films. Also, the increase in T_c that occurs when inert gases are added suggests that atomic hydrogen or protons are playing an important role, perhaps by means of an etching mechanism at the growing surface. As mentioned before, we found that T_c decreased from 400 to 370°C when the SiH_4 concentration was increased from 5 to 9%. However, increasing the SiH_4 content to 17% caused T_c to increase to $\sim$400°C again.

Changing the total pressure from 1.0 to 5.0 Torr, changing the flow from 55 to 110 SCCM, or changing the deposition-current density from 0.27 to 0.55 mA/cm^2 all had little effect on T_c ($\sim$370°C) for 9% SiH_4 (1.3% B_2H_4) in H_2. However, increasing the current density further to 1.1 mA/cm^2 decreased T_c to $\sim$350°C probably as a result of discharge-induced heating at the surface of the growing film. The thermocouple was located beneath the glass substrate.

Figure 3.3 (curve A) shows that a relatively low value of T_c ($\sim$265°C) was obtained with a discharge atmosphere containing SiF_4 and H_2 ($SiF_4/H_2 = 2$, $PH_2/SiF_4 = 5 \times 10^{-3}$). When the dopant source was from PH_3 to B_2H_6, deposition occurred only on the metal fingers and not on the glass. When a small amount of SiF_4 was added to a discharge containing 9% SiH_4 (1.4% B_2H_6) in H_2, so that $SiF_4/SiH_4 = 0.1$, T_c increased by only 10°C (Fig. C, curve B). However, increasing the SiF_4 content so that $SiF_4/SiH_4 = 0.3$ caused T_c to increase to $\sim$470°C (curve C).

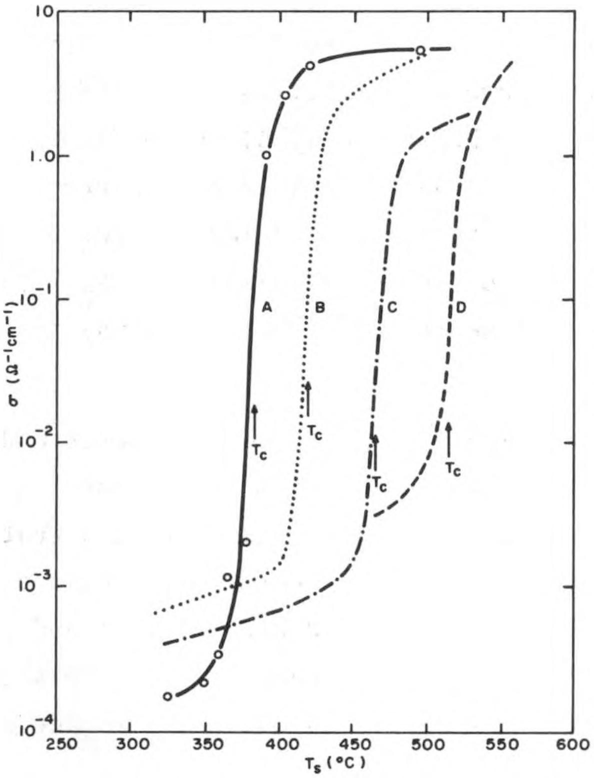

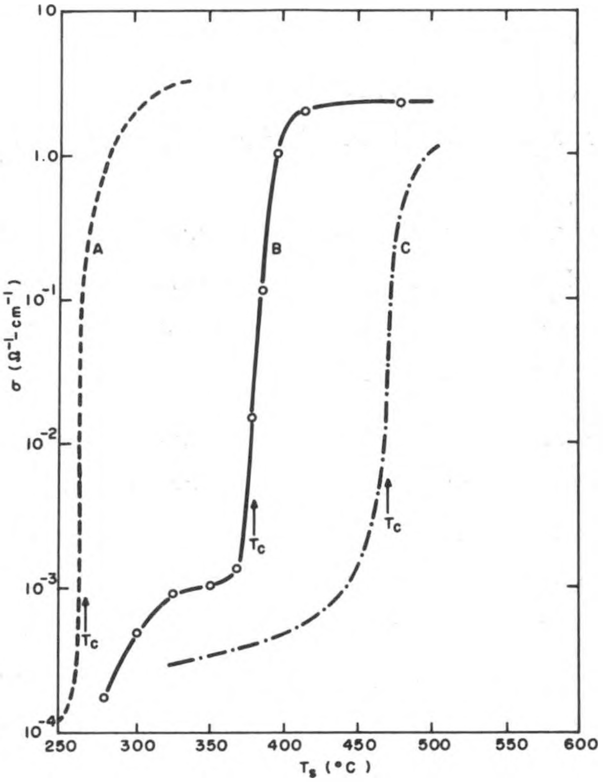

Figure 3-2. CONDUCTIVITY AS A FUNCTION OF SUBSTRATE TEMPERATURE FOR A SERIES OF FILMS GROWN IN VARIOUS DISCHARGE ATMOSPHERES (A: 5% SiH_4 (1% PH_3) in H_2; B: 5% SiH_4 (1.3% B_2H_6), 10% Ar, 85% H_2; C: 5% Si_2H_6 (1.5% B_2H_6) in H_2; D: 9% SiH_4 (1.3% B_2H_6) in H_2.)

Figure 3-3. CONDUCTIVITY AS A FUNCTION OF SUBSTRATE TEMPERATURE FOR A SERIES OF FILMS GROWN IN VARIOUS DISCHARGE ATMOSPHERES (A: $SiF_4/H_2 = 2$, $PH_3/SiF_4 = 5 \times 10^{-3}$; B: $SiF_4/SiH_4 = 0.1$, $B_2H_6/SiF_4 + SiH_4 = 1.4 \times 10^{-2}$ $SiF_4 + SiH_4/H_2 = 0.1$; C: same as B but $SiF_4/SiH_4 = 0.13$.)

Theses results indicate that SiF_4 increases T_c for boron-doped films. In the first case, the phosphorus atoms appear to act as nucleation sites for the formation of microcrystals [15]. Moreover, the presence of SiF_4 promotes an etching reaction that decreases the deposition rate, thus allowing more time for mobile species to increase the size of crystallites at the growing surface.

For p-type films grown in discharges containing SiH_4 diluted in H_2, the boron atoms may also act as nucleation sites, since T_c is only slightly higher (∿20°C than for similar phosphorus-doped films. However, the presence of SiF_4 inhibits the formation of p-type m-Si:H, probably due to the formation of boron-fluorine complexes. The boron-fluorine bond is very strong (∿8.07 eV) compared to the silicon-fluorine (∿5.64 eV) or silicon-hydrogen (∿3.26 eV) bonds [18].

SECTION 4.0

EXPERIMENTAL METHODS FOR CHARACTERIZING a-Si:H

4.1 THE DIFFUSION LENGTH OF HOLES IN UNDOPED a-Si:H

In Quarterly Report No. 1 we described our technique for measuring the minority-carrier diffusion length, L, in a-Si:H by the constant surface-photovoltage (SPV) method. We reported our first results, which yielded values of L between 0.3 and 0.4 μm and also showed that prolonged light-soaking resulted in a decrease in L that could be reversed by annealing. We now report measurements on a new set of samples with lower impurity content. We will focus on the dependence of L on light intensity, on temperature, on the effects of the previous thermal history of the samples, and on the beginning of a more thorough study of the effect of light-soaking on L.

Figure 4-1 shows the dependence of L on light intensity for a sample prepared at a substrate temperature, T_s, of 250°C. In these measurements, the independent variable was the constant surface photovoltage, ΔV, which was varied between 10 and 160 mV. However, it is more instructive to use as abscissa the quantum flux at one of the wavelengths used. We selected a λ of 6600 Å for this sample, where the penetration depth, $1/\alpha$, is 2.8 μm for a T_s of 250°C. The maximum intensity is thus slightly less than 0.1 Sun. We note that, at very low intensities of light, I, we obtain an L of 1.3-1.7 μm. As I is increased through four decades, L decreases to about 1 μm, remaining at this value between 10^{14} and 10^{16} q/cm^2 s. For the sample prepared at a T_s of 330°C, the results depend on the previous thermal history of the sample; there are two states (that we named "relaxed" and "metastable") that will be described here. In Fig. 4-2 we show the data for this sample in the relaxed state. Note that, at the higher light intensities, L remains essentially constant with a value of about 0.3 μm; at the lower intensities, L rises sharply to values greater than 1 μm. Figure 4-3 shows the results obtained on the same sample in the metastable state. Although the values of L at the lowest light level are the same as those in Fig. 4-2, we see that, at the highest light intensities, L is between 0.6 and 0.8 μm.

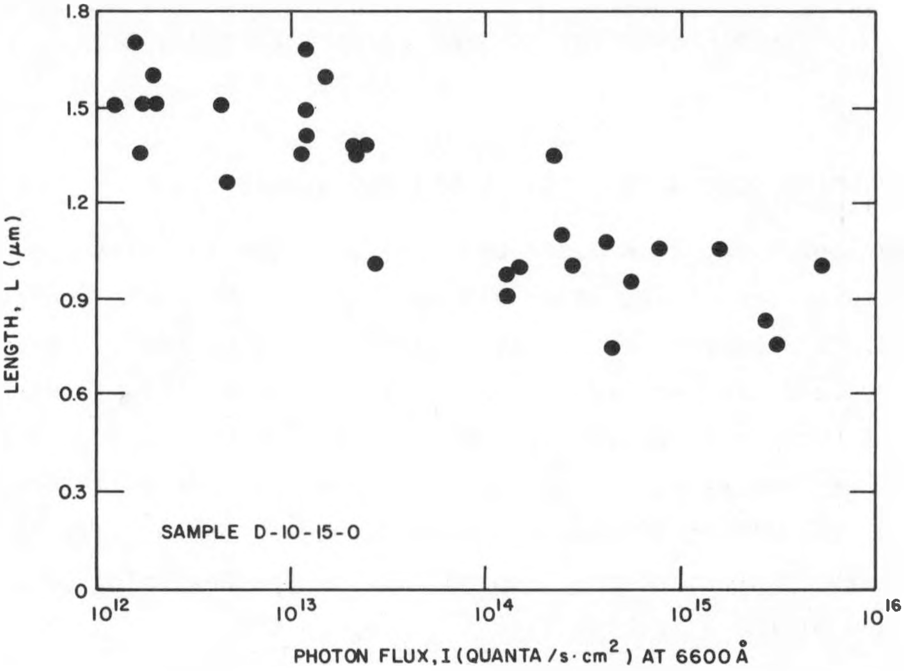

Figure 4-1. DIFFUSION LENGTH AS A FUNCTION OF LIGHT INTENSITY FOR AN a-Si:H FILM DEPOSITED AT 250°C IN A dc(p) DISCHARGE

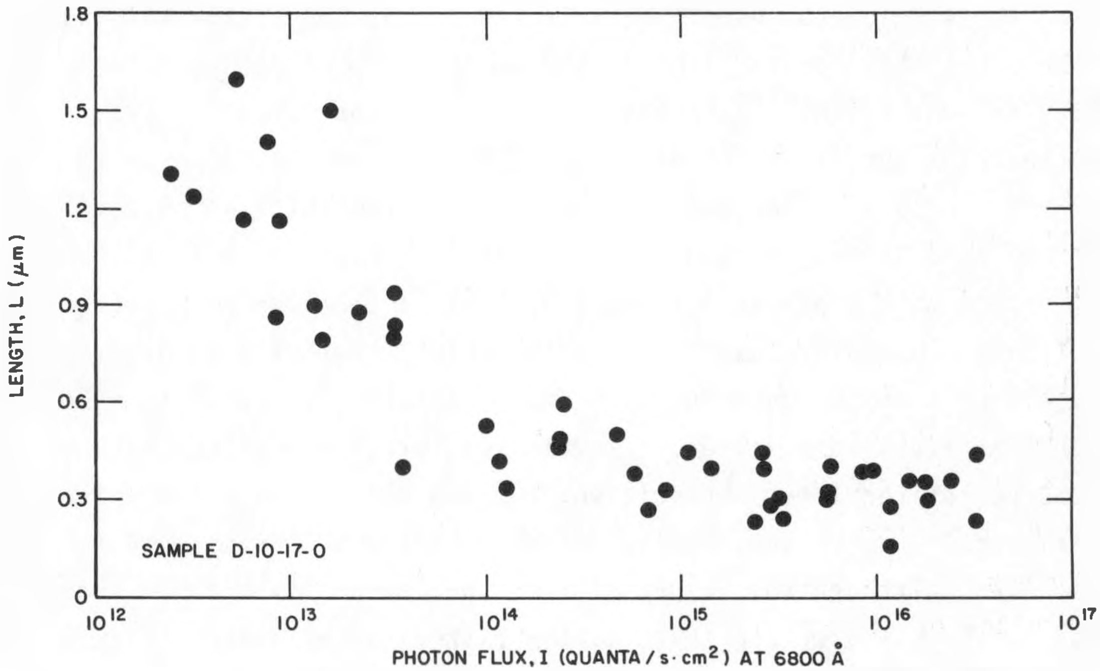

Figure 4-2. DIFFUSION LENGTH AS A FUNCTION OF LIGHT INTENSITY FOR AN a-Si:H FILM (deposited at 330°C) IN THE RELAXED STATE

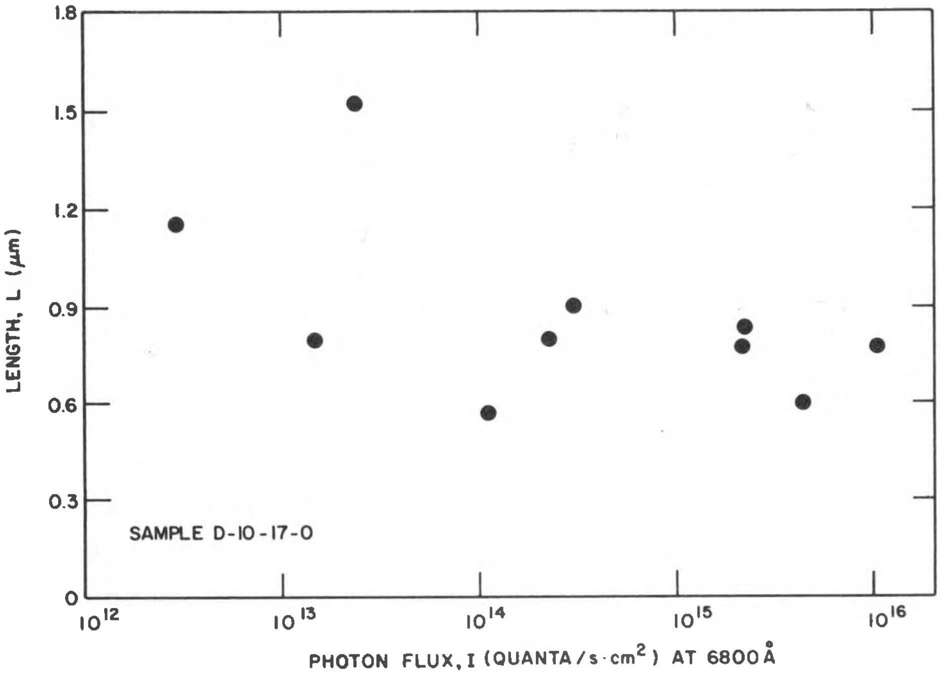

Figure 4-3. DIFFUSION LENGTH AS A FUNCTION OF LIGHT INTENSITY FOR THE a-Si:H FILM OF Fig. 4-2 IN THE METASTABLE STATE

The question arises whether our values of L, which are considerably larger than those reported by previous investigators, are true thermal diffusion lengths or rather field-assisted diffusion lengths (Schubweg). Figures 4-1 and 4-2 exhibit both of these situations. At very low light intensities, the depletion layer still extends appreciably into the sample and the surface field thus facilitates the collection of holes, in turn yielding an apparent value of L that is too large. At the higher light intensities the surface space-charge layer collapses. Capacitance measurements on Schottky-barrier cells on similar material (performed by A. Moore) show that, at 0.1 Sun, the depletion region has shrunk to less than 0.1 μm. A similar value can also be calculated from a knowledge of the carrier concentration under illumination in our samples. Thus, the independence of L over more than two decades of light intensity indicates that in the region of strong illumination we are measuring a true thermal-diffusion length, where $L = (D^2)^{1/2} = (\mu \frac{kT}{e} \tau)^{1/2}$. Some weaker evidence for this is given by the fact that the plots of I vs $1/\alpha$ in these experiments are linear. This implies either that there is no internal field in the sample or that any field is uniform throughout.

For the sample deposited at a T_s of 250°C, we found that its previous thermal history had no effect on L; however, the situation was different for the sample deposited at 330°C. We identified two states for this material, clearly characterized by different values of the diffusion length at the higher light intensities. One can cycle the sample repeatedly between the two states, always with the same result. A typical set of measurements of L at room temperature in the relaxed and metastable states is shown in Fig. 4-4. The "metastable" state, always yielding an L between 0.8 and 0.9 µm, is formed by heating the sample at about 50°C for 30 min and cooling it to room temperature. Once it is produced it is maintained even after a 15-min anneal at 200°C. The "relaxed" state, always yielding an L between 0.3 and 0.4 µm, is attained by keeping the sample more than three days in darkness. Strangely, once this state is attained, it is maintained after heating the sample to 200°C and slowly cooling it to room temperature. However, heating to 50°C for 30 min restores the metastable state. At present we can infer very little about this phenomenon; its lack of response

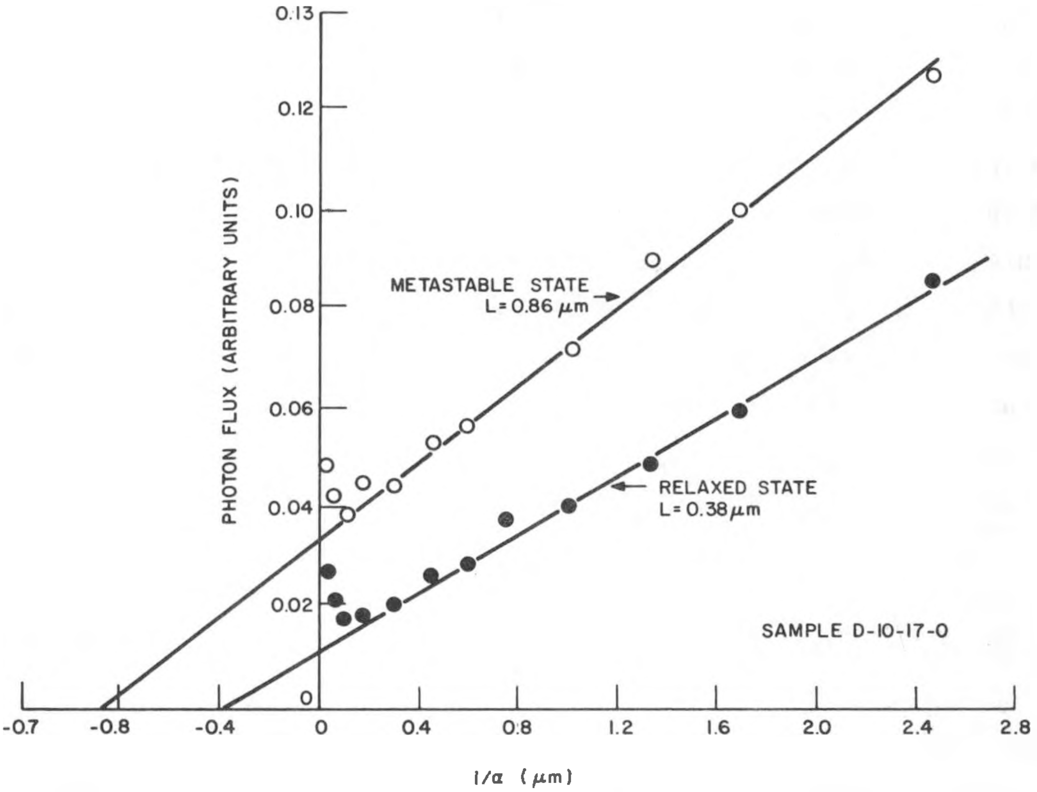

Figure 4-4. QUANTUM FLUX NECESSARY TO MAINTAIN CONSTANT SURFACE PHOTOVOLTAGE AS A FUNCTION OF α^{-1} at 330°C, WHERE α IS THE ABSORPTION COEFFICIENT

to annealing at 200°C suggests that very deep states may be involved. This phenomenon does not appear to be related to the light-soaking effects described below.

We measured the temperature dependence of L for both samples. Figure 4-5 shows the data obtained on the sample made at a T_s of 250°C; L exhibits an Arrhenius dependence with temperature with an activation energy, E, of 0.28 eV. A similar temperature dependence was found for the sample made at a T_s of 330°, for both the relaxed and the metastable state, and a value of 0.25 eV for E was obtained between -22 and 58°C. Measurements at higher temperature could not be made, because the SPV then becomes very small (due to surface recombination effect). The exponential dependence of L is probably related to the variation of the microscopic mobility with temperature, because the dependence of minority-carrier lifetime is expected to be very weak, as it is for crystalline Si. We have started some measurements of Hall mobility in very weakly doped p-type a-Si:H to verify this point.

Because of its practical importance in the operation of solar cells, we have continued our investigation of the effect of light-soaking on L. The behavior of the samples made at the two values of T_s is qualitatively similar: Both exhibit a decrease in the measured value of L and recover the original value upon annealing at 200°C. The results are the same if the light-soaking is done with white light or with uniformly absorbed light ($\lambda > 6200$ Å). However, measurements of L at different values of light intensity after light-soaking show that the $1/\alpha$ vs I data (such as in Figure 4-4) are often strongly nonlinear. This indicates that light-soaking has generated an internal field in the sample, probably by nonhomogeneous trapping of charge. So far we only have preliminary results. It may be that the decrease in L upon light-soaking is an apparent one, caused by this internal field, rather than the effect of a change in the transport parameters. The SPV method of measuring L may offer a new way of elucidating the nature of the Staebler-Wronski effect.

4.2 THE LIQUID SCHOTTKY-BARRIER METHOD FOR DETERMINING DIFFUSION LENGTHS

During the past quarter we have implemented another adaptation of the surface-photovoltage method of diffusion-length measurement in amorphous silicon. The

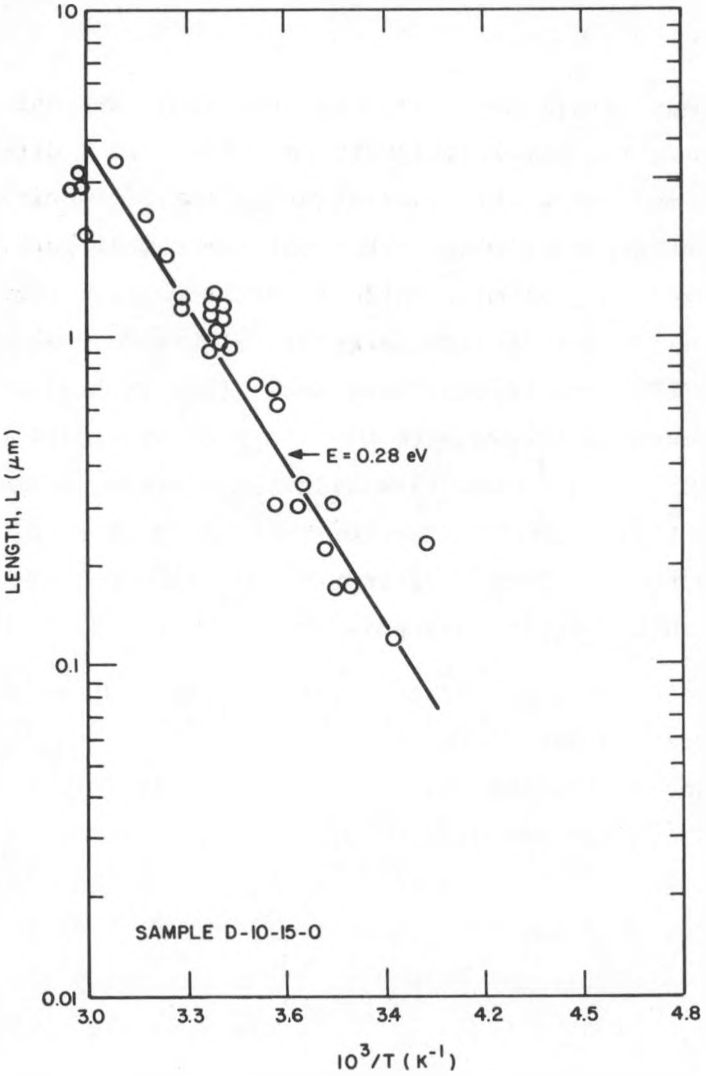

Figure 4-5. DIFFUSION LENGTH AS A FUNCTION OF $10^3/T$ FOR AN a-Si:H FILM DEPOSITED AT 250°C IN A dc(p) DISCHARGE

adaptation consists of the use of a liquid reduction-oxidation (redox) ionic couple as the surface contact. Such a solution, containing oxidizing and reducing ions, acts as a liquid Schottky barrier, with the barrier height determined by the redox potential. If, now, excess minority carriers are injected into the surface space-charge region of this Schottky-barrier system, the solution becomes biased to give an easily measured open-circuit voltage.

The minority-carrier injection is generally accomplished by illumination with light, the wavelength dependence of which gives the diffusion length of the carriers within the a-Si:H.

The advantage of this method over analogous measurements employing a Kelvin probe to find the surface photovoltage is that there is a direct conduction path to the source of potential. This eliminates all capacitive coupling, enabling either ac or dc measurement or a combination of both. The signals are large and almost noise-free down to signal levels of less than 1 mV. No surface preparation is necessary; no high-vacuum environment or elaborate shielding is required. A suitable redox liquid is simply placed in contact with the surface, and a platinum wire immersed in the liquid picks up the voltage. Naturally, there are disadvantages too. Some chemical action may take place, giving rise to a photovoltage even in the dark. R.Williams* showed that this could be minimized by loading the a-Si:electrolyte system electrically with about 1 MΩ of resistance, instead of maintaining a true open circuit. It is clearly impractical to make measurements over any appreciable temperature range, since the properties of the solutions would dominate all results. The solutions are usually colored, so the light transmission through the liquid must be taken into account. We have solved this problem by using a compensating solution of the same composition and thickness in front of the photodiode that measures the light intensity. Finally, we found that the principal disadvantage has nothing to do with fundamentals; some sample films on stainless steel simply break up when brought into contact with the liquid. When a break occurs in the film the liquid contacts the stainless steel substrate and the photovoltage is both shorted out (reduced in magnitude) and reacts much more slowly to the action of the light. These may be part of the same problem, but in any case, when the film is no longer continuous, the measurement fails. Some films seem very resistant to the liquid action, while others have broken up on contact.

We investigated a number of samples by the liquid Schottky-barrier method. The first few samples had previously been measured by the Kelvin-probe method. In several of these samples, particularly those with relatively low diffusion lengths, the results were in excellent agreement. In samples with longer

---

*RCA Laboratories.

diffusion length, we generally got results somewhat larger than those by the Kelvin method. This may be due to the generally lower signal level at which we work, combined with the observed sensitivity to high light levels. We intend to investigate this further, since the liquid Schottky-barrier approach is well suited to measurements as a function of total intensity.

Two large 7.6 cm X 7.6 cm samples were studied. In these, a temperature gradient was maintained in the substrate during the deposition. In the first sample (produced in an rf discharge), the substrate temperature ranged from 180 to 300°C. With no further annealing, the measurement indicated that the diffusion length varied almost linearly with substrate temperature, increasing from 0.2 μm at the cold end to 0.33 μm at the hot end. Clearly the higher temperature resulted in the best film.

In the second 7.6 cm X 7.6 cm sample (produced in a dc discharge), the temperature range was 270-400°C. Here we found that the measured diffusion length peaked at about 320°C, dropping sharply beyond 340°C. The maximum measured value was about 0.4 μm. The results of the two samples taken together are thus consistent: The intermediate temperature of near 300°C gave the best diffusion length. No doubt annealing will influence that result.

The surface-photovoltage method, whether used with the liquid Schottky barrier or the Kelvin probe, depends on the assumption of field-free drift. If a linear electric field is present over the region in which data are taken, it will act to give an effective "collection length" that will be larger than the true diffusion length for zero field. We normally use thick samples, so that we work well beyond the space-charge region. But if there are field lines from the front space-charge region to the rear space-charge region (i.e., if the space charge is not fully neutralized by surface double layers), the diffusion length will be overestimated. This remains to be investigated.

SECTION 5.0

FORMATION OF SOLAR-CELL STRUCTURES

5.1 PREPARATION OF a-Si:H CELLS FROM SiH_4-H_2 DISCHARGES

Following reports by Tawada et al. [2] we have begun exploring p-i-n cell preparation from glow discharges in 5-10% SiH_4 in H_2 at pressures from 0.5 to 1.0 Torr. The cell structure consists of glass/ITO/p-i-n/Ti/Al. Thus far we have found minor effects of rf power and of partial pressure of SiH_4 as well as the total pressure. A larger, inverse effect has been observed for the target-to-substrate separation (η = 3.8% for 5-cm and 4.3% for 2.8-cm separation). The largest effect has been observed upon removing a stainless-steel shield that contains the plasma. The absence of the shield drastically diminished the J_{sc}, FF, and η, but not the V_{oc}. We speculate that the shield confines and helps to bring to the target certain desirable gaseous species formed near the cathode. We are experimenting with improved confinement of the discharge.

In Table 5-1, we compare various p-i-n cells made in a SiH_4-H_2 glow discharge and having p layers in which CH_4 replaced some of the SiH_4 during the deposition. A distinct increase in J_{sc} is observed with increasing CH_4 content, as expected.

Table 5-1. PERFORMANCE DATA FOR A p-i-n CELL AS A FUNCTION OF C-CONTENT, WITH AM1 ILLUMINATION

$\frac{CH_4}{[CH_4 + SiH_4]}$	V_{oc} (mV)	J_{sc} (mA/cm^2)	FF (%)	η (%)
0	820	8.35	48	3.3
0.25	831	9.27	51	3.9
0.41	818	9.48	48	3.7

5.2 IMPROVED FRONT TRANSPARENT CONTACTS FOR p-i-n TEST CELLS

The ITO on glass presently in use is 62.5-mm thick and has a sheet resistivity of about 150 Ω/□. Hence, for even very small cells (~0.05 cm^2) tested at a reduced light level (~1/3 AM1) this sheet resistivity introduces substantial series resistance, R_s, at values of V_{oc} up to 5 Ω cm^2. This lowers the FF, J_{sc}, and η. In order to achieve fill factors of over 60%, the series resistance must be lowered either by the use of metal grids or by means of series-connected narrow cells. For rapid testing of many cells, the former is more practical. Hence, we made use of rf-sputtered Mo on ITO and etched "windows" in it (to define the cell areas) using photolithography and CF_4-O_2 rf plasma etching. Subsequently, a-Si:H p-i-n cells were deposited onto it and metal electrodes of Al sputtered on and etched to define areas greater than the windows. Films of Mo ~70-nm thick and having a sheet resistivity of ~2.5 Ω/□ were used, although in one case we tried a 380-nm-thick film (0.5 Ω/□) with fair success. For cell areas of 0.1 cm^2, we obtained FFs of 60% at 1/3 AM1 and 58% at AM1, with the type of cells showing an average FF of 55% at 1/3 AM1 without the grid. Significantly, R_s decreased by ~3 Ω cm^2 and was for the first time below 10 Ω cm^2. We found that we can coat 45 7.6 cm X 7.6 cm substrates per run with Molybdenum. The system is capable of up to 3 runs per day.

5.3 IMPROVED CELL EFFICIENCY BY MEANS OF REFLECTING METAL ELECTRODES

Because of the limited collection width in a-Si:H solar cells, the thickness of the cells is made smaller than would be required to absorb all useful light. Hence, it would be desirable to employ reflecting metal electrodes to make use of this excess light. Ondris and Den Boer [19] have reported that a thin Cr film plus a thick Ag film increases cell efficiencies 10-20% over those using Mo electrodes.

5.3.1 Al and Ti/Al Electrodes

From the standpoint of expense, aluminum would be a good alternative to a Cr/Ag electrode; however, we found aluminum to be unstable at elevated temperatures. Another alternative is thin Ti/thick Al.

We compared four sets of electrodes: thick Ti/Al, thin Ti/Al, rf-sputtered Al and thermally evaporated Al. The samples were also annealed for 1/2 hour in a an annealing-temperature, T_A, gradient from ~200 to 250°C (higher for Al). For as-prepared samples the V_{oc} for the first three electrodes was similar; for the evaporated Al it was about 30 mV higher. Regarding J_{sc}, the percentage increases over thick Ti/Al were as follows: for thin Ti/Al fill factors, 4.1%; for sputtered Al, 8.1%; and for evaporated Al, 6.4%. The fill factors (FF) for the first three were comparable, but for the evaporated Al the FF was about 11% lower.

Upon annealing, the V_{oc} for thick Ti/Al and thin Ti/Al increased up to 30 mV, but the FF suffered a large decrease with increasing T_A (from an initial FF of 56% to a final FF of 47-39%). For the evaporated Al the annealing over the T_A range severely impaired the cell performance. For the sputtered Al the damage began at ∿200°C and increased rapidly with T_A. I-V curves of as-prepared and annealed cells appear in Fig. 5-1. From these results it appears that an electrode consisting of Ti (5 nm)/Al (70 nm) is acceptable, but others should be sought for obvious improvements in V_{oc}, J_{sc}, FF, and stability.

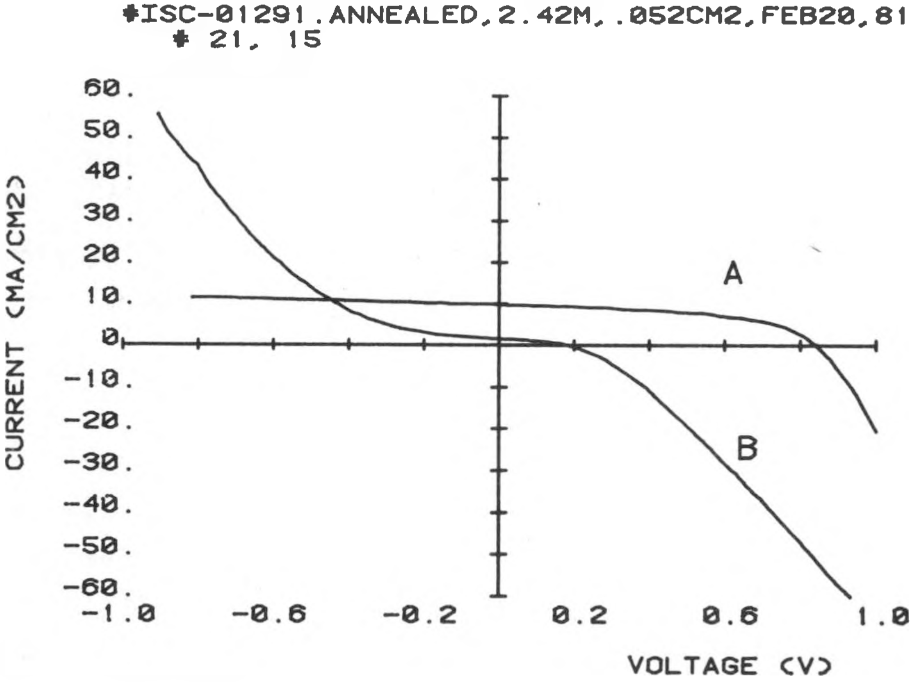

Figure 5-1. I-V CURVES FOR A p-i-n a-Si:H CELL HAVING AN EVAPORATED Aℓ BACK ELECTRODE (A: AS PREPARED; B: AFTER ANNEALING AT 267°C)

5.3.2 Indium Contact

Upon making routine measurements of V_{oc} by pressing solid In against the n layer of p-i-n cells, we measured values as high as 855 mV at 25% AM1 light. We found, however, that the values of V_{oc} thus measured are not necessarily reproduced with the Ti/Al contacts. In the case above they were lower by 50 mV. In another case V_{oc} increased from 818 to 830 mV. Apparently the n/metal interface is involved in this variation. The study of metal contacts is continuing.

5.4 COMPARISON OF OPTICAL STABILITY OF p-i-n CELLS MADE BY dc(p) AND rf(c) METHODS AND ILLUMINATED FROM p AND n SIDES

For over a year we have been studying two types of p-i-n a-Si:H cells -- those illuminated through the substrate and the p layer, and those illuminated through the film side and the n layer. For the purpose of elucidating some aspects of carrier transport and of optical stability, it was desirable to fabricate cells that could be illuminated from either side (p or n). The structure of these cells was glass/ITO/p-i-n a-Si:H/ITO. The p and n layers were nominally 10 nm thick; however, the effective p-layer thickness was much greater because of a graded rather than an abrupt junction. Samples were made by both the dc(p) and rf(c) methods and at a deposition temperature, T_s, of 280°C.

The measurements on the cells consisted of I-V curves under 16% AM1 light (because of high resistivity of the ITO) to obtain cell performance and collection efficiency, CE(λ). These tests were made from both sides and before and after a 68-h AM1 light-soaking (also from both sides). The test modes were:

A: tested from p-side, as-prepared state
B: tested from n-side, as-prepared state
A1: tested from p-side after light-soaking from p-side
A2: tested from p-side after light-soaking from n-side
B1: tested from n-side after light-soaking from p-side
B2: tested from n-side after light-soaking from n-side

The results of the I-V tests are shown in Table 5-2. Each test represents an average of 3 or more cells.

Table 5-2 PERFORMANCE DATA FOR p-i-n a-Si:H CELLS FOR VARIOUS MODES OF ILLUMINATION AND LIGHT SOAKING

Test Mode	Method	V_{oc} (mV)	J_{sc} (mA/cm^2)	FF (%)	η (%)
A	rf(c)	756	6.4	45	2.2
B	rf(c)	775	12.4	44	4.2
A1	rf)c)	724	6.9	42	2.1
A2	rf(c)	730	6.9	46	2.3
B1	rf(c)	739	10.1	38	2.8
B2	rf(c)	745	10.2	41	3.2
A	dc(p)	734	6.0	55	2.4
B	dc(p)	739	11.3	52	4.3
A1	dc(p)	701	5.9	48	2.0
A2	dc(p)	702	5.9	52	2.2
B1	dc(p)	712	9.4	40	2.7
B2	dc(p)	707	7.8	46	2.5

Representative results of CE(λ) are shown in Figures 5-2, 5-3, 5-4, and 5-5. The results can be summarized as follows:

Cells measured through the n layer (B) have higher η than those measured through the p layer (A) because of greater absorption in the p layer.

After light-soaking, cells measured through the n layer degrade more than cells measured through the p layer (compare B → B1, B2 with A → A1, A2). Degradation is not strongly influenced by the direction of soaking (compare A1 with A2 and B1 with B2). In degraded cells J_{sc} and FF decrease the most.

Figures 5-2 to 5-5 show the changes in the CE(λ) spectra on exposure. The CE(λ) measured through the n layer (Fig. 5-2) decreases by more than 60% in the blue (400 nm < λ < 550 nm) (Fig. 5-3), and only slightly in the red (λ > 600 nm). On the other hand, the CE measured through the p layer (Fig. 5-4) changes very little in the blue (Fig. 5-5). The relative change from 400 to 550 nm is clearly much less than for the n layer measurement and, in fact, shows a slight increase for the dc(p) cell.

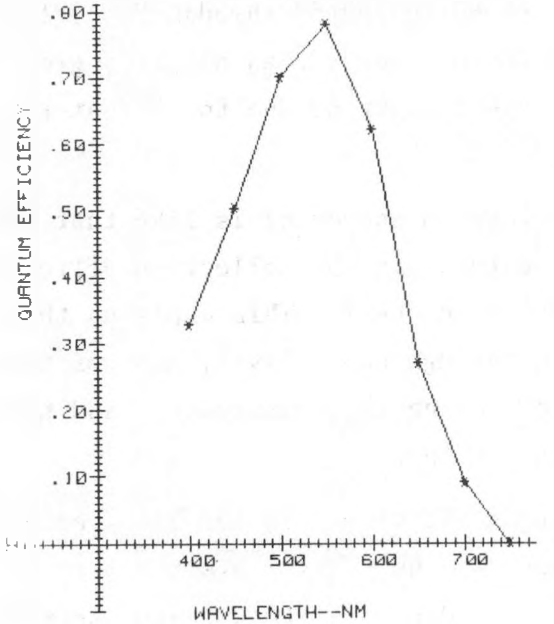

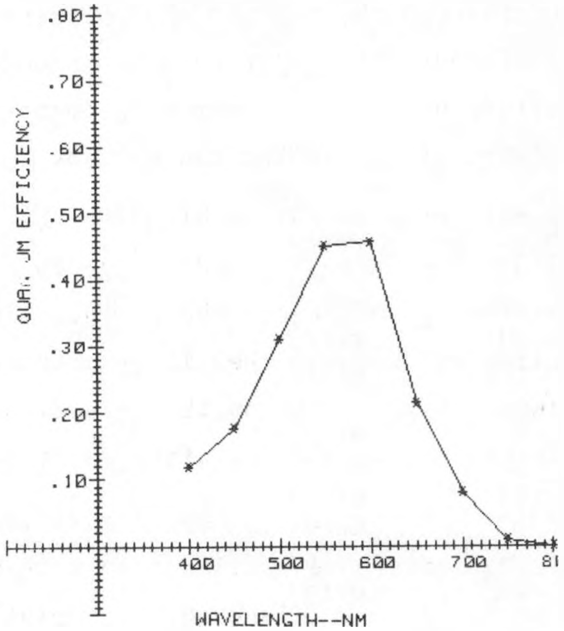

FIGURE 5-2. COLLECTION EFFICIENCY FOR AN AS-PREPARED CELL TESTED THROUGH THE n LAYER (TEST B) FIGURE 5-3. COLLECTION EFFICIENCY FOR A LIGHT-SOAKED CELL TESTED THROUGH THE n LAYER (TEST B2)

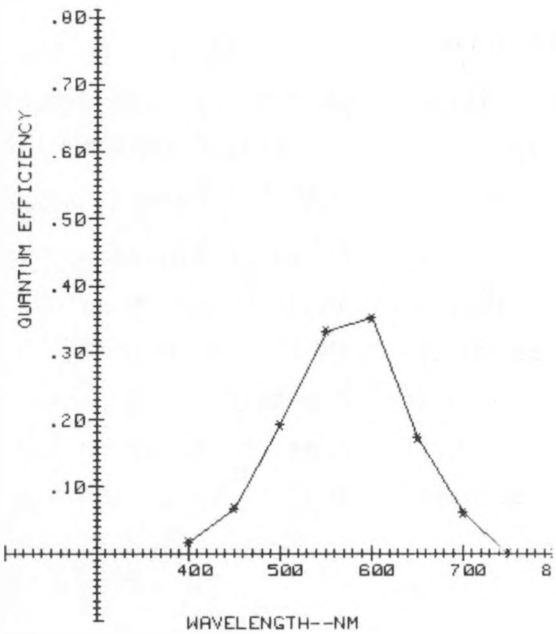

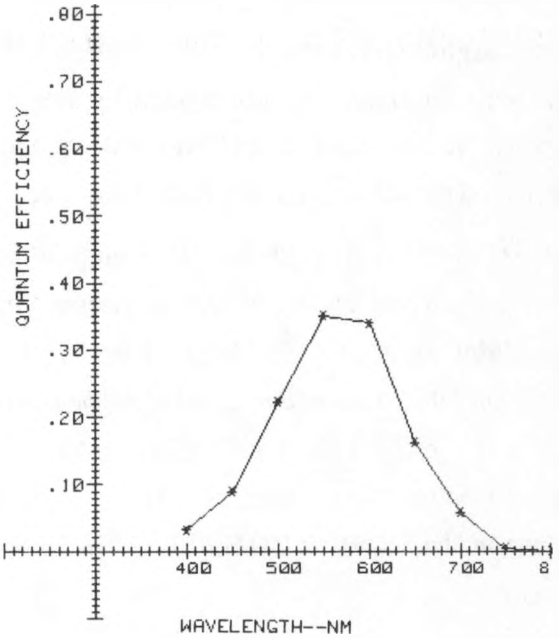

FIGURE 5-4. COLLECTION EFFICIENCY FOR AN AS-PREPARED CELL TESTED THROUGH THE p LAYER (TEST A) FIGURE 5-5. COLLECTION EFFICIENCY FOR A LIGHT-SOAKED CELL TESTED THROUGH THE p LAYER (TEST A2)

The direction from which light-soaking is done has a minor affect on cells tested through the n layer and no affect on cells tested through the p layer. In the former case light-soaking through the n layer causes slightly greater reduction in CE(λ) at lower wavelengths. This might be due to a greater integrated flux reaching the p layer.

The large decrease in the blue for the n layer measurement is like that seen for ITO/n-i-p/ss cells, and is due to a decrease in the collection efficiency of carriers generated on the n-layer side of the cell. This explains the stability of the cell when it is measured through the p layer; most of the carriers are generated on the p-layer side during the measurement, and these carriers are not strongly affected by degradation.

The p-layer measurement shows low collection efficiency in the blue, both before and after degradation. This is because the p layer absorbs more light than the n layer. (Although the nominal n- and p-layer thicknesses were 10 nm, the p layer was in fact thicker due to grading.) It accounts for the low efficiency found in p-layer measurements. From previous work we know that decreasing this absorption increases the efficiency. The work presented here suggests that better stability should be retained as well.

5.5 SIMS ANALYSIS OF A STABLE, rf-DEPOSITED p-i-n CELL

A p-i-n cell that improved from 2.8 to 3.5% upon light-soaking and thereafter remained stable has been SIMS analyzed. High contents of oxygen ($\sim 10^{21}$) and carbon ($\sim 10^{20}$) as well as a flat boron profile ($3\text{-}6 \times 10^{17}$) were surprising. The most probable reason for its stability is that the net i-layer thickness determined by SIMS appears to be only 0.25 μm, thin enough to be stable. There is no suggestion in these data as to the reason for improved efficiency on light-soaking.

SECTION 6.0

THEORETICAL AND EXPERIMENTAL EVALUATION OF SOLAR-CELL PARAMETERS

6.1 SOLAR-CELL INTERFACES

In an effort to assess the role of interfaces in a-Si:H solar cells, work-function differences between different exposed layers of the cells were measured in the dark and under illumination. Work-function changes under illumination (surface photovoltages) are attributable mainly to internal open-circuit photovoltages, rather than to surface band-bending changes [20]. Therefore, these measurements have been performed in room air, rather than in vacuum, using a noncontacting electrostatic millivoltmeter.

We measured the surface photovoltage of the exposed i layer on an i-p/ITO structure and obtained 0.2 V with uncalibrated white light. Since we had not detected any surface photovoltage for the exposed p layer on ITO, we conclude that, unlike the ITO/n interface [21], there is no significant barrier at the p/ITO interface. This result may be surprising for an interface that is equivalent to a p-n heterojunction. In this context it is worth mentioning that the properties of an interface formed between the same materials may still depend on the sequence of deposition, i.e., a p layer deposited onto ITO (p/ITO), and ITO deposited onto a p layer (ITO/p) may not necessarily form an identical interface.

6.2 EVALUATION OF ELECTROLYTE CONTACTS FOR IN-PROCESS TESTING OF SOLAR-CELL MATERIAL

It would be helpful if we could quickly test the quality of a-Si:H solar-cell material before final electroding. Ideally, this would give a good representation of the I-V characteristic of the final device.

A possible method would be to make use of an electrolyte contact. We would already have the n-i-p layer and need only make contact to the n layer. Reliable results can be obtained for V_{oc}, as discussed in Section 4.2. To get a full I-V curve involves a more difficult contact problem. Thin oxide layers form on the silicon and add a variable series resistance. However, the oxide can be removed with buffered HF. If measurements are then made quickly, with a solution of Cr^{+2}/Cr^{+3} ions as the active electrolyte species, short-circuit currents at quite a high level can be measured. For example, on an n-i-p structure, the J_{sc} was 7.0 mA/cm^2 in 1 Sun. Since there was no antireflection coating, this may represent the full current generated by the cell. On the same cell, V_{oc} was 0.72 V.

These may be good representations of J_{sc} and V_{oc}. The difficulty so far with this method is lack of reproducibility, i.e., variation from one part of the layer to another. (In a test procedure, any suspicion that the test itself may be incorrect is a lethal defect.) Some further experiments will be done to see if this can be brought under control. We believe some of the electrolyte is penetrating through microcracks or, possibly, through undamaged, but porous, material. This would give a variable electrochemical current from the steel substrate, superimposed on what we want to measure.

6.3 LOOKING AT SOLAR-CELL DATA STATISTICALLY

The most elementary statistical analysis can sometimes be helpful in showing what is really responsible for the differences in efficiency between one group of solar cells and another.

As an example, two groups, each consisting of data for ten cells, were picked from a large compilation of data for cells made in one discharge system. These were available as a computer printout arranged in order of decreasing efficiency. The first group consisted of the ten most efficient cells, with an average efficiency of 5.39%. The second group was a sequential series from farther down the list, with an average efficiency of 4.32%.

Table 6-1. AVERAGE PERFORMANCE VALUES FOR TWO GROUPS OF SOLAR CELLS

Group	Efficiency (%)	V_{oc} (mV)	FF (%)	J_{sc} (mA/cm^2)
1	5.39	807	0.53 ± 0.02	12.6
2	4.32	813	0.52 ± 0.02	10.2

Apparently, the factor determining the efficiency is J_{sc}. Other evidence indicates that the properties of the ITO and its contact to the a-Si:H are in control here.

SECTION 7.0

STABILITY STUDIES

7.1 PHOTON AND ELECTRON IRRADIATION EFFECTS

7.1.1 Photoluminescence and Annealing of Undoped a-Si:H

An undoped film of a-Si:H, deposited onto c-Si, was exposed to both laser and electron irradiation, and the resulting damage was compared on the same sample by photoluminescence and isochronal annealing. The photon dose was about 1 X 10^{22} photons/cm^2 at 500 nm, while the electron dose was about 1 X 10^{18} electrons/cm^2 at 5 keV. As observed previously, the photoluminescence intensity of the main peak at 1.2 eV degrades much more severely after electron irradiation (by about 90%) than after photon irradiation (by about 20%). Practically full recovery of the main peak is obtained with an identical annealing procedure in both cases. With regard to the photoluminescence at 0.8 eV, the photon exposure leads to an intensity increase by about 45%, while the electron exposure results in a decrease by about 80%. Photon exposure has always resulted in the 0.8 eV intensity increase [22] which is even more pronounced after irradiation above room temperature (about 100°C for the present sample). Electron irradiation, however, has previously led to either a decrease or an increase of the 0.8 eV intensity. The sensitivity of this 0.8 eV luminescence to temperature is borne out by the isochronal annealing of the present sample (see Fig. 7-1). The 0.8 eV intensity for the electron-irradiated area first recovers to its original value at a significantly lower annealing temperature than the main 1.2 eV intensity. Upon further annealing it increases to about 30% above its original value before it finally returns to its original value at about the same annealing temperature as the main peak. For the photon-irradiated area, the 0.8 eV intensity decreases monotonously to its original value, which is reached at the same annealing temperature as the main peak. Particularly from the properties of the 0.8 eV luminescence, we conclude that a temperature-assisted rearrangement of irradiation-affected bonds occurs.

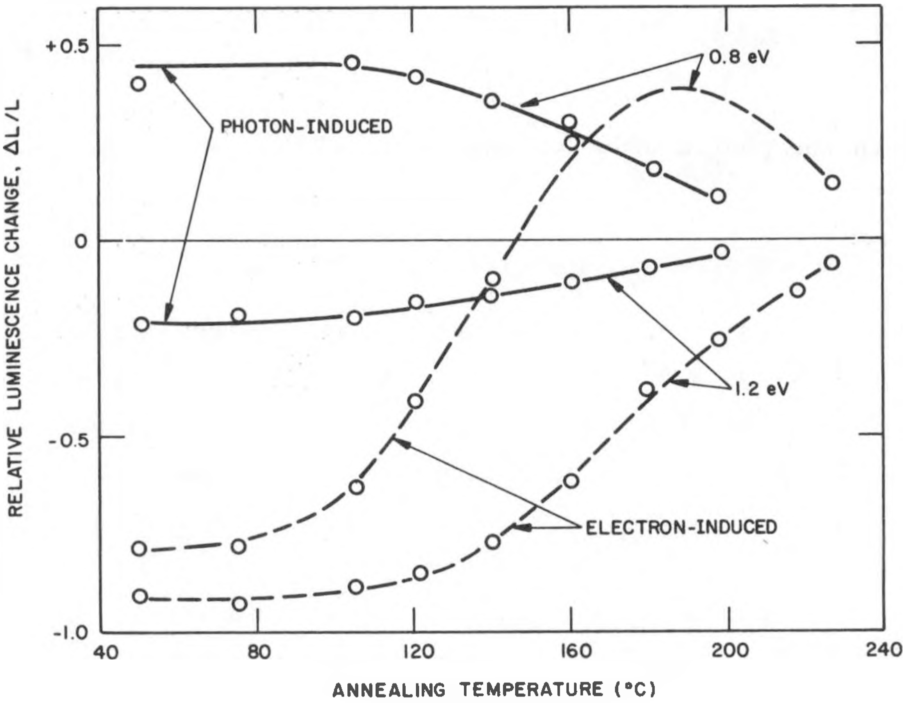

Figure 7-1. RELATIVE CHANGE OF PHOTOLUMINESCENCE INTENSITY AT 1.2 AND 0.8 eV AS A FUNCTION OF ISOCHRONAL (5 min) ANNEALING OF PHOTON-INDUCED AND ELECTRON-INDUCED IRRADIATION DAMAGE IN UNDOPED a-Si:H

7.1.2 Solar-Cell Properties

The similarities between photon-induced and electron-induced irradiation damage in a-Si:H suggest that electron irradiation might be applied as a means for accelerated life testing of solar cells. Unlike forward-bias degradation of solar cells, electron irradiation (and thus damage generation) can, like photon irradiation, be confined to a selected penetration depth. The evidence for similar types of damage due to photons or electrons would be greatly enhanced if cells known to be stable after light-soaking remain stable also after an equivalent dose of electron irradiation. Therefore, we are comparing finished cells after electron irradiation, known from light-soaking to be "stable" and "unstable." The electron penetration was chosen to reach through about half of the i layer. Table 7-1 shows the properties of a stable and an unstable cell before and after electron irradiation with a dose of 6 X 10^{15} electrons/cm^2, and then after annealing. The stable cell degraded to 0.96% efficiency, while the unstable cell degraded more -- to 0.77%. Both cells recovered practically to their original values.

The electron dose used in this experiment still exceeds a value that would be equivalent to the photon dose for the most unstable cells after 48 h of light-soaking. Exposure to still smaller electron doses is needed to check whether cells can be stable against both photon and electron irradiation. This would test the hypothesis that the type of damage, due to electrons and photons at equivalent doses, is the same.

Table 7-1. SOLAR-CELL PROPERTIES BEFORE AND AFTER ELECTRON IRRADIATION AND AFTER ANNEALING

(Irradiated with 6×10^{15} electrons/cm^2 at 6.2 keV)

	Stable Cell				Unstable Cell			
Status	V_{oc} (V)	I_{sc} (mA/cm^2)	FF (%)	η (%)	V_{oc} (V)	I_{sc} (mA/cm^2)	FF (%)	η (%)
Before e^-	0.82	12.37	0.53	5.35	0.79	12.10	0.54	5.14
After e^-	0.71	3.08	0.44	0.96	0.69	2.34	0.48	0.77
After Annealing	0.80	11.74	0.53	5.02	0.79	12.04	0.53	5.01

7.2 LIFE TESTS

One of our more stable cells (T09090), up to the time represented by this report, was exposed to simulated AM1 light for 3050 hours (nearly 20 weeks). The cell was kept biased at the maximum power point during illumination, and at a temperature around 40°C. It was completely unprotected from room ambient. Its efficiency is now 4.28%, down slightly from 4.4% at 2048 hours. The slow decay still follows the same straight line on the log-log plot shown in Fig. 7-2 of Quarterly Report No. 1 (SERI/PR-0-9372-1). Figure 7-2 shows this plot with the more recent data. Assuming that the daily average solar illumination is equal to 5 hours of AM1, this line predicts an efficiency above 4% after 10 years in sunlight.

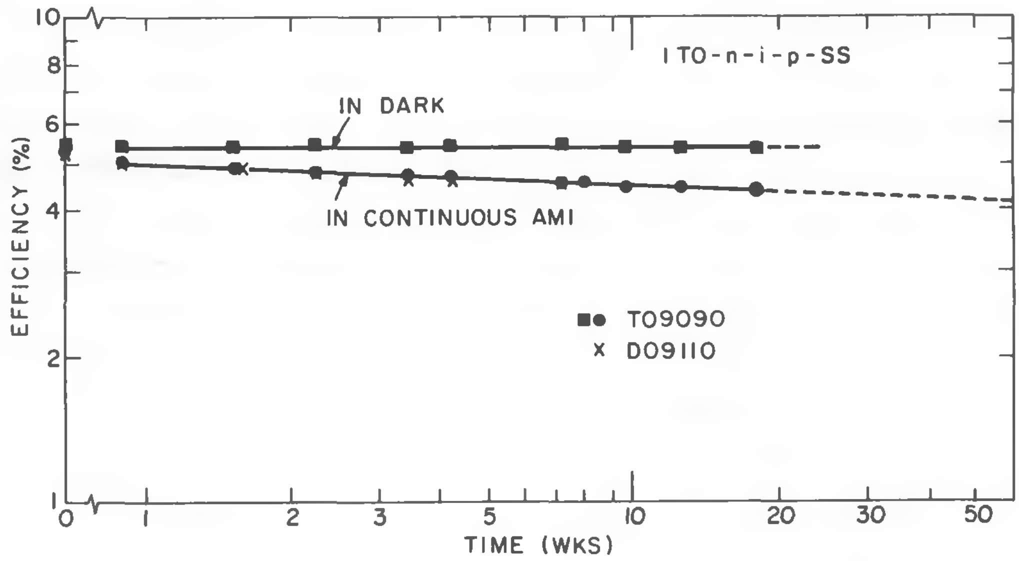

Figure 7-2. LIFE TEST RESULTS OUT TO 20 WEEKS FOR CELL T09090 (The upper curve is for a diode that was mashed from the light.)

7.3 CONDITIONS FOR STABILITY

We have been able to reproduce stable cells. Although the specific deposition or preparation conditions necessary for stability are not yet clear, we see some trends. The first is the boron profile in the i layer. The p layer is deposited first in these cells, from B_2H_6 added to the SiH_4. The rate at which the B_2H_6 is removed from the discharge, relative to the deposition rate of the i layer, determines the boron profile. Our results suggest that cells with a more graded profile have a higher probability of being stable. Another trend relates to the oxygen content. This was clearly shown in a series of cells deposited in an identical manner, but with different amounts of air bled in during the deposition of the i layer. With no air leak, the oxygen concentration was $\sim 2 \times 10^{20}$ cm^{-3}, and the cell was stable (it had a graded boron profile consistent with other stable cells). With maximum air bleed, the oxygen concentration was 2×10^{21} cm^{-3}, and the cell was unstable, even though its boron profile was approximately the same as before. We are continuing these studies to find out what role the boron profile and impurities such as oxygen are playing here.

7.4 DEGRADATION MECHANISMS

We have continued our tests on the degradation seen in unstable cells. The data in Fig. 7-3 establishes that the effects we see are not due to the light itself; they are caused by the free carriers the light generates. This figure shows the amount of decrease in the cell efficiency from a 48-h exposure to simulated AM1 illumination. It is plotted as a function of the voltage on the cell during the exposure. Maximum degradation occurs with the cell at V_{oc}. Decreasing the bias decreases the amount of degradation until, at the short-circuit state, the cell degrades about 1/3 of the value found for open-circuit degradation. Applying a reverse bias decreases the amount of degradation even more; at about -1 V, little or no change occurs.

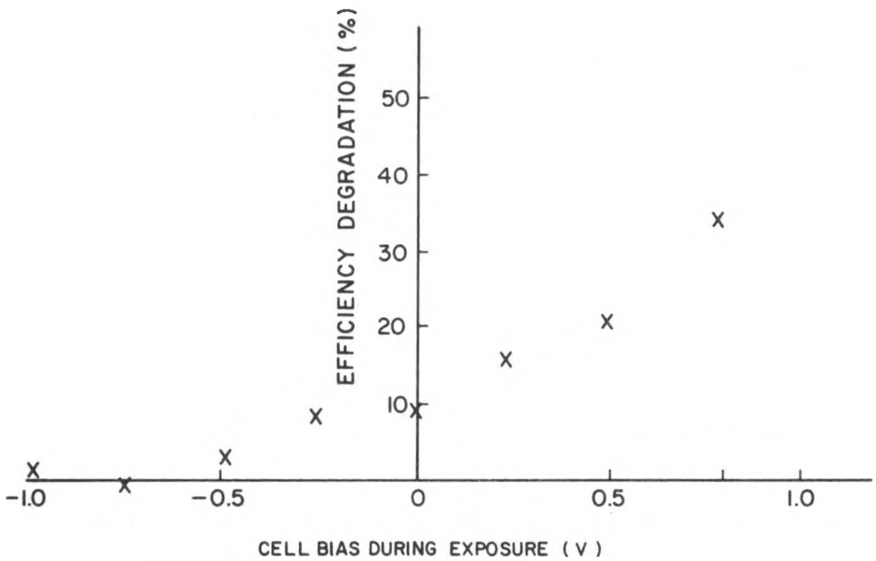

Figure 7-3. PERCENT DECREASE IN CELL EFFICIENCY AS A FUNCTION OF CELL VOLTAGE DURING A 48-h DEGRADATION IN SIMULATED AM1

The amount of light absorbed in each experiment is the same. The difference is how many optically generated free carriers have an opportunity to be trapped or recombine. At V_{oc}, most carriers are trapped or recombine inside the i layer. At reverse bias this is not true; most carriers are collected at the n or p layers. The conclusion is that the degradation is caused by a change in the i layer, and this change is created by trapping or recombination of free carriers.

Whether this causes a change in gap-state density or distorts the internal built-in field is not clear. Both can account for the measured degradation.

In the above model for degradation, the origin of the free carriers is not important. An important proof of this is that we can also degrade cells by applying a forward-bias current in the dark. The forward bias introduces free carriers that degrade the cell as in the optical degradation. The spectral changes are similar for the two types of degradation, and there is good correlation from sample to sample. A cell that is stable to optical illumination is also stable to forward-bias stressing.

To investigate the forward-bias stressing further, we degraded a number of similar cells under widely different forward bias. The cells were degraded for different times to keep the integrated charge (current X time) approximately the same. Table 7-2 shows the result. The data can be most easily understood by reference to Figure 7-4. The degradation effect has a threshold near flat-band voltage (where the built-in voltage is cancelled out), and is constant above that. The threshold effect suggests that minority carriers are involved, since current for applied voltage less than flat-band is predominantly from majority carriers.

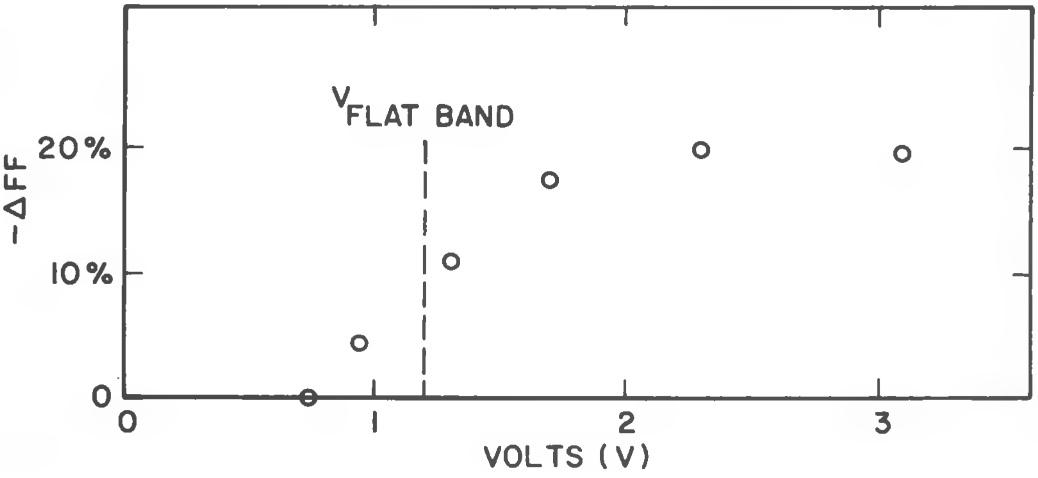

Figure 7-4. PERCENT DECREASE IN CELL FILL FACTOR AS A FUNCTION OF FORWARD BIAS

Table 7-2. DEGRADATION OF SOLAR CELLS AT VARIOUS LEVELS OF FORWARD-BIAS VOLTAGE

Voltage (V)	Current (mA)	Time (h)	I_t (mA-h)	ΔFF (%)
0.81	14	45	630	---
1.3	35	16.7	584	-11.2
1.7	90	6.7	603	-18.2
2.3	200	3	600	-20.4
3.1	500	1.1	550	-20.5

7.5 ACCELERATED TESTING

A disadvantage of our life tests is the time required to establish good stability (see Figure 7-2); an accelerated testing procedure is necessary. The standard technique of accelerating the degradation by heating the sample will not work here because of the annealing effects discussed in Section 7.6. New techniques are required. Two are discussed here: application of forward-bias current and exposure to high-intensity light.

Forward-bias accelerated testing is simple. One applies a forward-bias current in the dark, then measures the result with a standard I-V curve in the light. Table 7-2 shows the acceleration factor that can be achieved. Degradation similar to that found after 48 h of AM1 illumination can be done in only 1.1 h. This gives an acceleration factor of at least 45, so that a 20-yr sunlight test could be simulated in 5 wk. One possible problem, however, is the high currents used in the test: up to 500 mA for a ~1.19 cm^2 cell. This is much higher than the current the cells were designed for in AM1 operation; thus, voltage drops in the transparent contact (ITO, in this case) may lead to a large spatial nonuniformity in degradation. We are in the process of measuring the nonuniformity with laser scanning. If it is indeed severe, a special cell may have to be designed for use in this accelerated-testing method.

Exposure to high light intensities is another possible approach. The problem here is to keep the light from overheating the cell. Small cells on metal substrates are most suitable. Figure 7-5 shows an example for a 0.095 cm^2 n-i-p cell on a stainless-steel substrate. The cell was continually exposed to a ~6 W/cm^2 beam of red laser light (λ = 676 nm). The change in cell photocurrent, monitored with a weak, blue laser beam, was rapid and reached saturation in ~10 min. Although this specific test has not been carried out in simulated AM1 (monitoring the blue response as a function of time), these results suggest an acceleration factor of more than 100. We will continue these tests with laser beams and high-intensity white-light sources. Our aim is to find a practical and rapid test for stability.

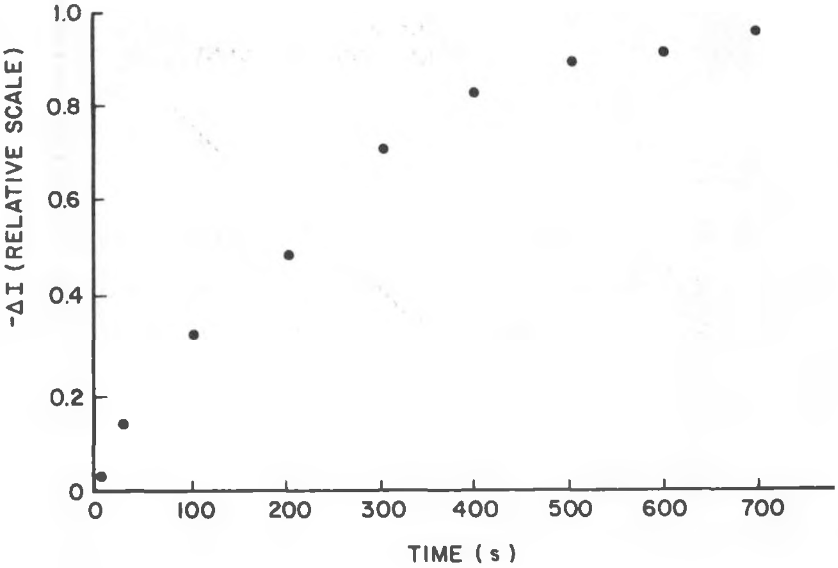

Figure 7-5. CHANGE IN THE BLUE PHOTORESPONSE OF A CELL (ΔI) DURING EXPOSURE TO A 6-mW/cm^2 LASER BEAM (λ = 676 nm)

7.6 THERMAL ANNEALING

A degraded cell is in a metastable state; it remains that way for weeks if stored in the dark at room temperature. However, heating it to 200°C for ∿1/2 h returns it to its original condition. This process has been repeated many times in one cell, with no sign of fatigue, and appears to be completely reversible.

Heating a cell to 300°C also reversibly anneals it. Heating it to 100°C produces only a partial effect; the efficiency doesn't return to its original value. Some preliminary checks suggest an activation energy of ∿0.8 eV for the annealing process. Figure 7-6 shows the results for decay of degradation induced by forward-bias current. Here the degradation and annealing were done at the same temperature. Checking a similar cell at 200°C showed that the decay-time constant of a cell degraded in light at room temperature was ∿300 s, a factor of three higher than that shown on Figure 7-6.

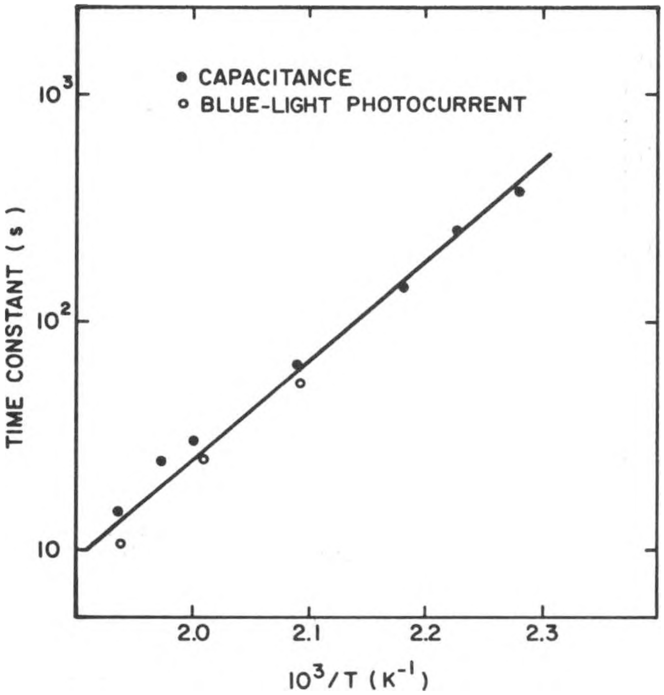

Figure 7-6. DECAY TIME CONSTANT FOR CAPACITANCE AND PHOTOCURRENT VALUES AS A FUNCTION OF INVERSE TEMPERATURE (The slope gives the activation energy.)

SECTION 8.0

REFERENCES

1. D. E. Carlson, Solar Energy Materials 3, 503 (1980).
2. Y. Tawada, T. Yamaguchi, L. Nonomura, S. Hotta, H. Okamoto, and Y. Hamakawa, The 2nd Photovoltaic Science and Engineering Conf. in Japan (1980).
3. A. Madan, J. McGill, W. Czubotyj, J. Yang, and S. R. Ovshinsky, Appl. Phys. Lett. 37, 826 (1980).
4. D. L. Staebler, in W. Paul (ed.), Proc. 8th Int. Conf. on Amorphous and Liquid Semiconductors, Cambridge, MA, August 27-31, 1979, in J. Non-Cryst. Solids 36-36, 387 (1980).
5. C. R. Wronski, D. E. Carlson, and R. E. Daniel, Appl. Phys. Lett., 29, 602 (1976).
6. A. Rose, Concepts in Photoconductivity and Allied Problems, Interscience, New York (1963).
7. H. Fritsche, Solar Energy Materials 3, 447 (1980).
8. S. M. Sze, Physics of Semiconductor Devices, Wiley-Interscience, New York (1969), p. 370.
9. R. S. Crandall, R. Williams, and B. Tompkins, J. Appl. Phys. 50, 5506 (1979).
10. Ref. 9, p. 107.
11. A. Rothwarf, private communication; V. Dalal, private communication.
12. C. R. Wronski and R. E. Daniel, Phys. Rev. B23, 794 (1981).
13. R. Williams and R. S. Crandall, RCA Review 40, 37 (1979).
14. A. R. Moore, Appl. Phys. Lett. 37, 327 (1980).
15. A. Matsuda, S. Yamasaki, K. Nakagawa, H. Okushi, K. Tanaka, S. Iizima, M. Matsumura, and H. Yamamoto, Japan J. Appl. Phys. 19, L305 (1980).
16. S. Usui and M. Kikuchi, J. Non-Cryst. Solids 34, 1 (1979).
17. Y. Nagata, A. Kunioka, and S. Yamazaki, Appl. Phys. Lett. 38, 142 (1981).
18. Handbook of Chemistry and Physics, Chemical Rubber Co., c1966, p. F130.
19. M. Ondris and W. Den Boer, Proc. of the 3rd E. C. Photovoltaic Solar Energy Conf., Cannes, France, Oct. 1980, p. 809.

20. D. E. Carlson, I. Balberg, R. S. Crandall, J. Dresner, B. Goldstein, J. J. Hanak, H. E. Schade, D. L. Staebler, and H. A. Weakliem, Quarterly Report No.1, SERI/PR-0-9372-1 prepared for the Solar Energy Research Institute under Subcontract No.XG-0-9372-1, February 1981.
21. B. Goldstein, D. Redfield, D. J. Szostak, and L. A. Carr, to be published in Appl. Phys. Lett.
22. J. I. Pankove and J. E. Berkeyheiser, Appl. Phys. Lett. 37, 705 (1980).
23. J. Reichman, Appl. Phys. Lett. 38, 251 (1981).
24. W. Shockley and W. T. Read, Phys. Rev. 87, 835 (1952).

APPENDIX A

DERIVATION OF ELECTRIC FIELDS OF THE p-i-n STRUCTURE

The electric fields in the p-i-n structure depicted in Fig. 2-6 can be readily derived by standard methods. We make the assumption that the i-layer thickness is fixed at a length L and the n and p layers are thick enough so that they do not become fully depleted under reverse bias. The n layer contains positive space charge of density ρ_+; the p layer contains negative space charge ρ_-. The depletion widths in these layers are W_+ and W_- for the n and p layers, respectively.

Because of the growth procedure for the p-i-n cell, the i layer is expected to be graded p to n type from the p-i interface. Therefore, it is reasonable to represent the space charge in the i layer by negative charge decreasing away from the i-p interface. The space-charge densities are assumed uniform in the p and n layers.

Poissons equation in the three regions are thus

$$\frac{dE_n}{dx} = \rho_+/\varepsilon \ , \tag{A-1}$$

$$\frac{dE_p}{dx} = -\rho_-/\varepsilon \ , \quad \text{and} \tag{A-2}$$

$$\frac{dE_i}{dx} = -\rho_-\left(\frac{x}{x_c}\right)^\alpha \frac{1}{\varepsilon} - \rho_s/\varepsilon \ . \tag{A-3}$$

where the subscripts on the electric field, E, refer to the different layers. The coordinate system is chosen with x = 0 at the i-n interface and x = L at the i-p interface. A power law with exponent α was chosen for the space-charge gradation in the i layer. There is also a uniform space charge of density ρ_s in the i layer.

Integration of Eqs. A-1, A-2, and A-3 gives

$$E_n = \rho_+ \ (x - w_+)/\varepsilon \ , \tag{A-4a}$$

$$E_p = -\rho_- \, (x + w_-)/\varepsilon \text{ , and} \tag{A-4b}$$

$$E_i = \rho_- \, L \left(\frac{x}{L}\right)^{\alpha+1} / (\alpha + 1) - \rho_s \, x/\varepsilon + E_o \quad . \tag{A-4c}$$

The depletion widths and the uniform part of the field in the i layer are found by matching the fields at the boundaries. Integration of Eqs. A-4a and A-4b and, again, the use of the boundary conditions, permits all the constants to be expressed in terms of V_o, the potential difference across the structure.

After some algebraic manipulation, the constant field in the i layer can be determined in terms of the potential and the space-charge densities. However, the expression is rather unwieldy in its general form. Since the experimental conditions are usually such that the space-charge gradient is large in the i layer and, furthermore, the impurity density ρ_s is much less than the doping in the p and n layers, E_o can be approximated by

$$E_o = V_o/(1 - b)L - L\rho_s/\varepsilon \quad , \tag{A-5}$$

where $b = \rho_s Ne$. This expression shows that as long as the average field, V_o/χ_o, in the i layer is greater than the surface-field, $L\rho_s/\varepsilon$, due to the space charge in the i layer, the field in the i layer is approximately uniform.

The depletion width, W, for this structure is given by

$$W = L + W_+ + W_- \quad ,$$

$$= L \, \xi \left[1 + \frac{4}{\xi^2 L^2} \left(\frac{\xi \, L^2}{(\alpha + 1)(\alpha + 2)2\varepsilon} + V_o \right) \frac{\varepsilon}{2\rho} \left(\frac{1}{N_D} + \frac{1}{N_A} \right) \right]^{1/2} \quad , \tag{A-6}$$

where $\xi = \alpha/(\alpha + 1)$, and N_D and N_A are impurity densities in the n and p layers, respectively. In the limit of small α, the uniform density of space charge in the i layer, $W \, \alpha \, \sqrt{V_o}$, and the p-i-n cell would behave like a Schottky-barrier cell. In the opposite limit, where $\alpha >> 1$ and the doping density decreases rapidly away from the p-i interface, the depletion width is

$$W \approx L \left[1 + \frac{\varepsilon}{e} \left(\frac{1}{N_D} + \frac{1}{N_A} \right) \frac{V_o}{L^2} \right] \quad , \tag{A-7}$$

which shows a linear change in depletion width with voltage, in agreement with the data in Fig. 2-7.

APPENDIX B

APPROXIMATE SOLUTION OF COUPLED-CONTINUITY AND POISSON EQUATIONS FOR THE p-i-n STRUCTURE

An exact analytical solution of the coupled-continuity and Poisson's equations may not be possible for the p-i-n structure. Apart from the difficulty resulting from the coupling of Poissons equation to the continuity equations through the free-carrier space charge, the problem of the strong spatial dependence of the free-carrier lifetimes makes an exact solution difficult. This spatial dependence of the lifetimes results from the fundamental condition that the electrons and holes must recombine in pairs, so that their respective recombination rates are equal at all points in space. Stated mathematically this condition is

$$\frac{n(x)}{\tau_x(x)} = \frac{p(x)}{\tau_p(x)} . \tag{B-1}$$

Reference to Fig. 2-9, which is a sketch of the electron and hole density in the i layer, shows that, near the blocking contacts, n and p have strong variations with distance from the contacts. Because of the above condition on the recombination rates, this will result in a strong variation in the lifetimes.

Nevertheless, we can arrive at an approximate solution of the system of Poissons and the continuity equations that can give physical insight into the transport in the p-i-n structure. Surprisingly enough, this approximate solution agrees well with experiment. First, we simplify the problem by taking the electric field across the i layer to be uniform. This was discussed in the text and shown to be a good assumption. Second, we restrict the solutions to those for uniformly abosrbed light. Under these conditions diffusion can be neglected [23]. This simplifies the algebra somewhat. Under these conditions the set of equations to be solved is

$$-v_p \frac{dp(x)}{dx} + G - \frac{p(x)}{\tau_p(x)} = 0 \quad , \tag{B-2}$$

$$v_n \frac{dn(x)}{dx} + G - \frac{n(x)}{\tau_n(x)} = 0 \quad . \tag{B-3}$$

The boundary conditions for these equations are that the minority carriers vanish at the blocking contacts. This means that the hole density vanishes at the n-i interface, which is blocking for holes, and, similarly, the electron density vanishes at the p-i interface. Therefore,

$$p(o) = n(L) = 0 \quad . \tag{B-4}$$

As discussed above, these equations cannot readily be solved because of the lack of knowledge of the x dependence of the lifetimes. An expression for the lifetime that might apply to the p-i-n structure is that derived from the Schockley-Read [24] recombination theory. However, the solutions of Eqs. B-2 and B-3 that result from the use of this theory are mathematically complex and it is difficult to obtain physical insight from the solutions. Therefore, we chose to make the following approximations to $\tau_n(x)$ and $\tau_p(x)$ to permit straightforward solutions of these equations. Actually, the Schockley-Read recombination theory shows that the approximate expressions for the lifetimes are reasonably valid where they are applied. We separate the i layer into three regions and make approximations to the lifetime in the different regions that permit solutions of the continuity equations. The natural separation is into the two regions near the contacts, where transport determines the carrier densities, and a bulk region, where recombination determines the carrier densities.

In region 1 near x = 0, where the hole density is zero, $p(x)/\tau_p(x)$ can be neglected with respect to G. Thus Eq. B-2 becomes

$$v_p \frac{dp(x)}{dx} = G \quad . \tag{B-5}$$

With the boundary condition (Eq. B-4), the solution of this equation is

$$p(x) = G\, x/v_p \quad , \tag{B-6}$$

which is a hole density that increases linearly from the n-i interface. Current continuity requires that the electron density in this region will also have a linear variation, with x reaching a maximum at x = 0.

Similar considerations apply in region 3, near x = L at the p-i interface. Here $n(x)/\tau_n(x) << G$, so that the approximate solution of Eq. B-3 is

$$n(x) = G(L - x)/v_n \quad . \tag{B-7}$$

In region 2, in the bulk, both $n(x)/\tau_n(x)$ and $p(x)/\tau_p(x)$ are on the order of G. Thus the drift term in the continuity equations can be neglected, and the electron and hole densities are given by the usual expressions in photoconductors,

$$n = G\,\tau_n \quad ; \quad p = G\,\tau_p \quad . \tag{B-8}$$

In this region the lifetimes are constant, independent of x, so that $\tau_n(x) = \tau_n$ and $\tau_p(x) = \tau_p$.

As long as region 3 is less than the i-layer thickness, L, the current will be ohmic and given by Eq. A-1. With increasing electric field, region 2 shrinks, and finally recombination is unimportant throughout the i-layer; a saturated photocurrent results.

The above arguments reproduce the general features of the current-voltage curve in Fig. 2-1. However, it is desirable to connect the two limits of strong recombination and ohmic-current flow with the regime of a saturated photocurrent. This can be accomplished in a reasonable way if we make the lifetimes of the minority carriers constant over the transition region between the bulk and the surface regions. After finding the solutions we will see that this approximation is better than it appears at first glance. With this approximation the solution of Eq. B-2 is

$$p(x) = G\tau_p[1 - \exp(-x/l_p)] \quad . \tag{B-9}$$

This solution has the proper limits in regions 1 and 2. In region 1, when x is small, it reduces to Eq. B-6. When x is much larger than the hole drift length, lp, (region 1) then Eq. B-9 reduces to Eq. B-8. Of course, we expect this solution to be reasonable in the region of strong recombination, because the lifetime is constant under these conditions.

Similar considerations can be used to find an expression to connect regions 2 and 3. It is

$$n(x) = G\tau_n[1 - \exp((x-L)/l_n)] \quad . \tag{B-10}$$

The above approximate expressions for n and p will not both be correct solutions of the continuity equations for all x values. In fact there is only one value, x_c, at which both solutions satisfy the continuity equations. This point is found by demanding that dJ/dx be zero, using Eqs. B-9 and B-10 for the current. The critical x value is

$$x_c = \frac{L}{(1 + l_n/l_p)} \tag{B-11}$$

For values of $x < x_c$ the electron density is found by substituting the hole density given by Eq. B-9 into the first integral of the continuity equations, which is

$$J = e[v_n n(x) + v_p p(x)] = ev_n n(o) = ev_p p(L) \tag{B-12}$$

Similarly for $x > x_c$ the hole density is found by substituting Eq. B-10 into Eq. B-12. The total current, J, is found by substituting Eqs. B-10 and B-9 into Eq. B-12 and evaluating the expression at $x = x_c$. The result is

$$J = eG\left(l_n + l_p\right)\left[1 - \exp\left(\frac{-L}{l_n + l_p}\right)\right] \tag{B-13}$$

It now remains to show that the assumption of a uniform field throughout the i layer is a reasonable one. To show this we calculate the field distortion due to the free-carrier space charge by means of Poisson's equation

$$\varepsilon \frac{dE(x)}{dx} = e\left(p(x) - n(x)\right) \quad , \tag{B-14}$$

where ε is the dielectric constant. Instead of calculating the field distortion in general, we shall calculate it for the worst case; that is, when there is no recombination and the mobility of one carrier is much larger than the other. Since, in this regime the space charge is inversely proportional to the drift velocity, the slow carrier contributes the majority of the space charge. If $\mu_p << \mu_n$ then

$$\Delta E(x) = \frac{eG}{Gv_p}\left(\frac{x^2}{2}\right) \quad , \tag{B-15}$$

where $\Delta E(x)$ is the field distortion. As the condition on the amount of field distortion, we calculate the fractional change in voltage due to this distortion

$$\text{Error} = \frac{\int_0^L \Delta E(x)dx}{V_o} = \frac{1}{6}\frac{e\ G\ L^4}{\varepsilon\mu_p V_o^{\ 2}} \quad , \tag{B-16}$$

where V_o is the applied voltage. As an example let the absorbed photon intensity correspond to a short-circuit current of 0.012 A, the i layer be 5×10^{-5} cm, μ_p be 10^{-2} and V_o be 1 V. Then Error = 0.025, which is indeed small. Even though the error increases as V_o decreases, it will not become as large as Eq. B-16 predicts, because the space charge decreases under conditions of strong recombination.

☆U.S. GOVERNMENT PRINTING OFFICE: 1981-740-145/2602